Aus dem Institut für Neurophysiologie
der Medizinischen Fakultät Charité – Universitätsmedizin Berlin

DISSERTATION

NMDA-receptor inhibition and oxidative stress during hippocampal maturation differentially alter parvalbumin expression and gamma-band activity

zur Erlangung des akademischen Grades

Doctor of Philosophy (PhD)

vorgelegt der Medizinischen Fakultät
Charité – Universitätsmedizin Berlin

von

Luisa Austin Hasam Henderson

aus Mexiko Stadt, Mexiko

Datum der Promotion: 06.09.2019

Table of contents

Abbreviations

APV- (2R)-amino-5-phosphonovaleric acid

Au - Auranofin

BSO - Buthionine sulfoximine

Cch - Carbachol

DIV - Days *in vitro*

GABA - Gamma-aminobutyric acid

GAD67 - Glutamate decarboxylase 67

GSH - Glutathione

mCBI - Monochlorobimane

MK-801 - Dizocilpine

MWU - Mann Whitney U test

NMDAR - N-methyl-D-aspartate receptors

Nrf2 - factor-erythroid 2-related factor 2

P - Postnatal day

PCP - Phencyclidine

PNNs - Perineuronal nets

PV - Parvalbumin

ROS - Oxygen radical species

Trx - Thioredoxin system

VGAT - Vesicular GABA transporter

4AP - 4-aminopyridine

Zusammenfassung

Es gibt immer mehr Hinweise dafür, dass frühe postnatale Störungen in neuronalen Netzwerken zur Pathologie der Schizophrenie beitragen. Veränderungen in neuronalen Netzwerken, vor allem in Parvalbumin (PV) exprimierenden schnell feuernden Interneuronen des präfrontalen Kortex und des Hippokampus sowie abnormale Gamma-Band Oszillationsaktivität, werden mit Schizophreniesymptomen, sowie kognitiven Störungen und Verhaltensauffälligkeiten, assoziiert. Genetische und entwicklungsbedingte Risikofaktoren sind Teil eines gemeinsamen Mechanismus, der eine Hypofunktion des NMDA-Rezeptors (NMDAR) und ein Redox-Ungleichgewicht beinhaltet. Ihre Auswirkungen auf die Entwicklung von neuronalen Netzwerken wurden im Einzelnen noch nicht untersucht.

Die Verwendung organotypischer, hippokampaler Schnitt-Kulturen, in denen sich die elektrophysiologischen Eigenschaften der PV-positiven, schnell feuernden Interneuronen *in vitro* ausbilden, erlaubt es, die Effekte der NMDAR-Inhibition und des oxidativen Stresses auf Gamma-Oszillationen und PV-Expression unabhängig voneinander zu untersuchen. Um diese jeweiligen Effekte zu analysieren, haben wir entweder das Gluthation- (GSH), Peroxidedoxin/Thioredoxin-Antioxidanz-System partiell blockiert oder die NMDAR inhibiert. Sowohl die NMDAR-Inhibition als auch die GSH-Blockierung induzieren Proteinoxidation, unterdrücken PV-Expression und verändern durch Carbachol induzierte Gamma-Oszillationen, obgleich in unterschiedlicher Weise. NMDAR-Inhibition führt zu einer sofortigen Reduktion der Gamma-Oszillations-Frequenz, gefolgt von einer Unterdrückung der PV-Expression. Im Gegensatz dazu führt die GSH-Blockierung zu einer sofortigen Verminderung der PV-Expression und erhöht die Oszillations-Amplitude ohne die Frequenz zu beeinflussen.

Bemerkenswerter Weise führt die Verstärkung der neuronalen Netzwerkaktivität mittels des Kalium-Kanalblockers 4-Aminopyridine zu einem ähnlichen Effekt wie die Blockade der NMDAR in Bezug auf die Gamma-Oszillation, jedoch ohne die PV-Expression zu beeinflussen. Zudem steigert 4-Aminopyridine die Überlebensrate der Interneurone.

Die Veränderungen der PV-Expressionen und abweichende Gamma-Oszillationen werden bei Schizophrenie häufig zusammen beobachtet, könnten anhand unserer Ergebnisse jedoch unabhängige Komponenten der Krankheitspathologie repräsentiere

Abstract

An increasing amount of evidence suggests that early postnatal disturbances in neuronal network development might underlie the pathology of schizophrenia. Alterations in neuronal circuitry, particularly affecting the parvalbumin- (PV) expressing fast-spiking interneurons in the prefrontal cortex and in the hippocampus, as well as abnormal gamma-band oscillatory activity, have been associated to schizophrenia-related cognitive and behavioral symptoms. Genetic and developmental risk factors of this pathology converge on a common mechanism involving NMDA receptor (NMDAR) hypofunction and redox imbalance, yet their individual impact on developing neural circuitries has not been assessed.

Using organotypic hippocampal slice cultures, where the electrophysiological properties of the PV-positive fast-spiking interneurons maturate *in vitro*, allowed to independently study the effects of NMDAR-inhibition and oxidative stress, elicited by partial blockade of the glutathione (GSH) and the peroxiredoxin/thioredoxin antioxidant systems, on gamma oscillations and on PV expression.

Both NMDAR inhibition and GSH depletion induced protein oxidation, suppressed PV expression, and altered carbachol-induced gamma oscillations, albeit in a different manner. NMDAR inhibition led to an immediate reduction in the gamma oscillation frequency, followed by suppression of PV expression. In contrast, GSH-depletion immediately decreased PV expression and increased the power, without affecting the frequency. Remarkably, enhancement of neuronal network activity by the potassium channel blocker 4-aminopyridine mimicked the effect of NMDAR inhibition on gamma oscillations without affecting PV expression and promoting interneuron survival. Hence, although changes in PV expression and aberrant gamma oscillations are observed in schizophrenia, they could represent independent components of the disease.

1. Introduction

1.1 Schizophrenia and gamma-band oscillations

Schizophrenia is a chronic and debilitating neuropsychiatric disorder affecting ~ 1 % of the world's population. The psychopathological manifestation of this disorder comprises positive (delusions and hallucinations), negative (impaired emotional processing and social withdrawal), and cognitive (impaired working memory) symptoms with an onset in early adulthood. Despite continuous efforts, the available treatments are mainly effective in ameliorating the positive symptoms, while the handling of negative and cognitive symptoms remains a challenge (1, 2, 3). Cognitive and perceptual processing is believed to arise from the synchronized oscillatory activity within and between neural networks (4, 5). Particularly, oscillations in the gamma-band (30-130 Hz) have been shown to be relevant for higher cognitive functions (4, 6, 7). In schizophrenia patients, disturbances in the power and frequency of these oscillations, in response to stimuli or during cognitive tasks, have been reported in EEG and MEG studies (6, 7). Furthermore, in animal models of the disease, alterations in gamma-band activity in the prefrontal cortex and hippocampal formation have been associated to cognitive deficits as well as behavioral changes comparable to those observed in the pathology of schizophrenia (8, 9). Thus, aberrant gamma-band activity is currently believed to underlie the cognitive clinical manifestations, representing a therapeutic target and a potential biomarker of the disease (4, 7).

1.2 Gamma oscillations and the role of parvalbumin-positive basket cells

Local gamma oscillations are generated by the interplay between glutamatergic pyramidal neurons and perisomatic inhibitory basket cells. In particular, gap junction-coupled interneurons expressing the calcium-binding protein parvalbumin (PV) exert rhythmic control on the principal cell output thereby synchronizing neuronal ensembles during gamma activity (10, 11, 12, 13). The critical involvement of these interneurons in shaping neural oscillations has led to the hypothesis that disturbances in GABAergic transmission might mechanistically underlie the network desynchronization, resulting in cognitive deficits. Indeed, decreased expression of the GABA-synthesizing enzyme GAD67 and GABA membrane transporter GAT1 in PV+ basket cells is a common finding in postmortem specimens from schizophrenia patients, hinting at aberrant inhibition and probable deregulation of pyramidal cell activity (8, 14, 15, 16). In addition to decreased GAD67 and GAT1, loss of PV expression has been reported in hippocampal and cortical basket cells –a finding that has been reproduced in animal models of this disease (8, 16, 17, 18).

1.3 NMDA receptor hypofunction in schizophrenia

It has been suggested that the impaired GABAergic neurotransmission observed in schizophrenia arises from the abnormal glutamatergic signaling mediated by ionotropic N-methyl-D-aspartate receptors (NMDAR). NMDAR blockade using phencyclidine (PCP) or ketamine was shown to exacerbate the positive and negative symptoms of schizophrenia patients while mimicking them in healthy controls (20, 21). Furthermore, NMDAR antagonism is known to induce activity disturbances in the gamma-band range (22). Also, lower expression levels of the NMDAR obligatory subunit NR1 (glycine binding site) have been reported in postmortem brain samples of patients, while alterations in genes related to glutamatergic transmission and synaptic plasticity have been associated to increased schizophrenia susceptibility (23, 24). In animal models, NMDAR hypofunction induced by genetic or pharmacological means results in behavioral changes, cognitive deficits and aberrant gamma-band oscillations along with reduced expression of GAD67 and PV, similar to that observed in the pathology of schizophrenia (7, 25, 26, 27).

Dysfunctional NMDAR during neuronal development have been shown to be particularly deleterious, as the activity of these receptors is critically involved in neuronal survival, migration, as well as synaptic refinement and maintenance (28, 29). Although NMDAR are present in both pyramidal and GABAergic cells, postnatal interneuron-specific NMDAR ablation is enough to induce loss of PV and GAD67 expression and to disturb cortical oscillations, as well as hippocampal synchrony (27, 30). Thus, NMDAR hypofunction during early development might particularly influence the neuronal network by interfering with the interneuron function (28).

1.4 Oxidative stress and the glutathione system in schizophrenia

Environmental insults occurring around birth (prenatal infection, malnutrition, obstetric complications and stress), acting together with genetically predisposing factors, have been suggested to contribute to the progression of schizophrenia by inducing oxidative stress (29). Disturbance of the antioxidant defenses in schizophrenia patients, in particular decreased levels of the small molecular antioxidant glutathione (GSH), have been reported in tissue, plasma, and cerebrospinal fluid (31, 32, 33). Furthermore, treatment with N-acetyl-cysteine (Nac), a precursor of GSH synthesis, has been shown to ameliorate the cognitive symptoms (34, 35). In animal models, mutations in the GSH-synthesizing enzyme resulted in PV loss, decreased power of gamma oscillations, and behavioral symptoms resembling this pathology (36, 37). Moreover, pharmacological depletion of GSH led to altered plasticity, suggesting an impact of

GSH on NMDAR function (38). However, NMDAR dysfunction might be also upstream of the oxidative stress. In the model of ketamine-induced acute psychosis, loss of the fast-spiking phenotype of PV+ basket cells was dependent on the activation of the superoxide-producing enzyme NADPH-oxidase 2 (39, 40), while alterations resulting from NMDAR hypofunction following ventral hippocampus lesion were prevented by the antioxidant Nac (37). Thus, aberrant network function in schizophrenia is hypothesized to result from the interplay between NMDAR hypofunction and redox dysregulation (25).

1.5 PV-positive basket cells and oxidative stress

The increased susceptibility to perinatal oxidative stress and NMDAR hypofunction reported for PV+ basket cells has been associated to their protracted maturation. These interneurons develop their electrophysiological and electrochemical properties, as well as PV expression, over the first postnatal weeks (41, 42, 43, 44), a period during which alterations might have the greatest impact on network function. Additionally, PV itself works as a metal-dependent antioxidant (45) and it emerges concurrently to the formation of perineural nets (PNNs). PNNs are high-density extracellular molecules that enwrap PV+ interneurons, exerting protective effects against oxidative insults and limiting plasticity and synaptogenesis (46). However, PNNs are themselves susceptible to oxidative stress and their degradation can lead to altered synaptic connectivity (47). In postmortem studies of human schizophrenia patients, reduced PNN labelling has been reported for several brain regions (48, 49, 50).

Furthermore, PV+ basket cells might themselves produce a high free radical load. These fast-spiking interneurons generate narrow action potentials at high frequencies, implicating large metabolic rates (51, 52) –this is also reflected in their particularly elevated content of cytochrome C (53). Moreover, the development and modulation of the function of antioxidant systems is regulated by NMDAR activity. Thus, hypofunction of these receptors can result in weakened antioxidant defenses (25, 54, 55, 56, 57). Hence, altered PV+ basket cell maturation resulting from dysfunctional detoxification mechanisms and/or environmentally-induced subliminal oxidative stress might underlie the aberrant oscillatory patterns observed in schizophrenia (3, 53, 58).

2. Objective

Perinatal NMDAR hypofunction and oxidative stress share common consequences such as suppression of PV expression of basket cells and appearance of aberrant gamma oscillations. However, the contribution of these factors to the pathological alterations, as well as the causal

link between them, are unknown; NMDAR hypofunction can by itself induce oxidative stress, whereas oxidative stress might disturb NMDAR function. In my thesis, I sought to test the individual effects of NMDAR hypofunction and oxidative stress on hippocampal slice cultures, where the interneurons and the neuronal network develop *in vitro* under controlled conditions. I have hypothesized that during neuronal maturation NMDAR inhibition and GSH depletion would both reduce PV expression and alter the properties of carbachol-induced gamma oscillations, whereas enhancing spontaneous synaptic activity would contribute to the PV+ interneuron and network development. Furthermore, characterizing a model where the neuronal network develops *in vitro*, as well as the contribution of NMDAR inhibition and GSH depletion to its maturation, could advance the understanding of the pathological processes underlying schizophrenia.

3. Materials and methods

3.1 Organotypic hippocampal slice culture preparation

Animal care and handling was in accordance with the Helsinki declaration and institutional guidelines. Slice culture preparation was approved by the State Office of Health and Social Affairs, Berlin (license number T0123/11).

Hippocampal slice cultures were prepared according to the Stoppini method (59) using rats expressing the yellow fluorescence protein Venus under the promoter of the vesicular GABA transporter (YFP-VGAT) (60), allowing the identification of interneurons. Rats were decapitated at postnatal day (P) 6-7, the brains were extracted under sterile conditions and collected in ice-cold minimal essential medium (MEM). By performing a sagittal incision, the two hemispheres were separated and the section containing the hippocampal formation, the subiculum and the entorhinal cortex was dissected from each hemisphere. The extracted hippocampal-entorhinal cortex complexes were placed on sterile filter paper and cut coronally into 400 μm slices by using a McIllwain Tissue Chopper (Mickle Laboratories, Guildford, UK). The slices were flushed with ice-cold MEM and collected in a petri dish. Slices displaying a complete and undamaged hippocampal formation were seeded in pairs in 0.4μm/30mm diameter Millipore Millicell culture plate inserts (Millipore, Eschborn, Germany). The inserts were placed on 6-well multidishes (Multidish 6, NUNC GmbH & Co. KG, Wiesbaden, Germany), each well containing 1 ml of warmed medium (50% MEM, 25% HBSS, 25% Horse Serum from Gibco, Eggenstein, Germany), supplemented with 1 mM Glutamax (Gibco, Eggenstein, Germany). Slices were cultured for as long as 15 days in an incubator maintained

at 36 °C/ 5% CO_2 (61, 62, 63, 64, 65). The medium was replaced 3 times per week. For each slice preparation session, 2 to 4 rats were used.

3.2 Pharmacology

Three lines of pharmacological treatments were included in this study: NMDAR inhibition, oxidative stress, and enhanced synaptic activity. 1) NMDAR inhibition was achieved by exposing slice cultures to DL -2-Amino-5-phosphonopentanoic acid (APV) (50 μM, Tocris), a selective NMDAR antagonist. 2) Oxidative stress was induced by a simultaneous partial blockade of the GSH and the thioredoxin (Trx)-dependent antioxidant systems, by inhibiting the rate-limiting enzyme of GSH synthesis (gamma-glutamylcysteine synthetase) with L-Buthionine sulfoximine (BSO 1μM, Sigma-Aldrich), and by applying auranofin (Au), a blocker of the thioredoxin reductase enzyme. The blockade of the Trx system was included in the treatment since it is known to compensate for GSH deficits (66, 67). 3) Enhanced synaptic activity was induced by exposure to the blocker of voltage-gated K^+ channels, 4-Aminopyridine (4AP) (100 μM, Tocris). The treatments started at DIV1 by applying the drugs to the medium and were refreshed with every medium change. Slices were processed for experiments at DIV3, 10, or 15. These time points were selected based on the characterization of the *in vitro* maturation of fast-spiking interneurons (68, Hasam-Henderson *et al.*, 2018). In the process of establishing the aforementioned protocols, different BSO (0.5, 5 and 10 μM) and Au (0.5, 5 and 10 μM) concentrations were evaluated.

3.3 Local field potential recordings of gamma oscillations

For the induction and measurement of gamma oscillations, slices were carefully cut out from the membrane inserts and placed on Haas-type recording chambers perfused with warmed gassed artificial cerebrospinal fluid (aCSF) (34°C, 95 % O_2 , 5 % CO_2, 1.3 ml per minute) containing (in mM) : NaCl 129, KCl 3, NaH_2PO_4 1.25, $MgSO_4$ 1.8, $CaCl_2$ 1.6, $NaHCO_3$ 26, glucose 10, pH 7.3). Glass micropipettes with a resistance lower than 4 MΩ were filled with aCSF and placed in the CA3 pyramidal layer. Measurements were performed on slices at DIV3, 10, and 15. For the recordings an EXB-EXT-02B NPI Electronic amplifier (NPI, Germany), high-pass filtered at 0.1Hz, low-pass filtered at 1 kHz, and sampled at 5 kHz by a digitizer CED Micro1401-2 with a ADC12 extension (Cambridge Electronic Design Limited, Cambridge, UK) were used. Hippocampal slices were recorded for 8000 s; for induction of gamma oscillations carbachol (Cch) (5 μM) was administered via the perfusion at 1000 s and was present for the rest of the recording.

3.4 Immunocytochemistry

For immunolabelling, slice cultures at different culturing stages (DIV3, 10, and 15) and acute slices at ages P0 and P21 were fixed overnight in a solution of 4% PFA /4% sucrose, followed by a minimum of 12 h storage in a PBS 1x/30% sucrose solution. Slice cultures were then detached from the membrane inserts using a thin brush and both acute slices and cultures were processed free-floating. Slices were incubated for three nights with an anti-parvalbumin antibody (1:1000, mouse-derived, Millipore) in 1% Triton X-100 and for one night with a Cy3 secondary antibody (1:100, goat anti-mouse, Millipore). Slices were washed with PBS between protocol steps. Finally, slices were mounted on gold-coated slides (Vectrashield HardSet Mounting Medium) and stored at 4 °C. A similar staining procedure was carried out for the labelling of perineuronal nets using biotinylated wisteria floribunda lectin (1:500, Vector Laboratories, USA), followed by incubation with Streptavidin-Cy3 (1:100, Invitrogen, USA).

3.5 Image acquisition and analysis

Image acquisition was performed with either a spinning disk confocal microscope (Andor Revolution, BFIOptilas GmbH, Gröbenzell, Germany, objectives 20x, NA. 0.5 and 60x NA. 1) or with a NIKON A1R MP multiphoton microscope (Nikon, Amsterdam, The Netherlands, objective 25x N.A. 1.1). In both cases, 30 to 80 focal planes per field of view were acquired with a distance of 1.2 µm. Three-dimensional reconstructions of the complete hippocampal formation were used to quantify the absolute numbers and the ratio of YFP+ and PV-labelled interneurons. Images taken with the spinning disk confocal microscope were arranged into hippocampal panorama images (69) and maximal projection images were processed using ImageJ-Fiji (Madison, Wisconsin, USA) (*Analyze Particles* plugin and *Cell Counter* plugin, Wayne Rasband, NIH). Panorama images automatically acquired with the multiphoton microscope were analyzed using Arivis Vision 4D (Blobfinder analysis operator, Arivis AG, Unterschleissheim, Germany) and ImageJ (*Cell Counter* plugin). Slice thickness varied greatly depending on the time in culture and the applied treatment. These variations, together with the uneven slice-top reliefs resulting from unconfined growth in culture, made it necessary to introduce a normalization protocol to objectively analyze the changes in the PV expression and in the hippocampal interneuron population. Two data representations were adopted: 1) number of YFP+ interneurons and number of PV+ per image stack; these values were calculated by dividing the number of YPF+ and PV+ interneurons per slice by the number of imaged z-planes and, 2) a ratio of YFP+/PV+ interneurons per slice presented as percentage. For every treatment and time point, 10-20 slices obtained from 3-10 rats were imaged and analyzed. Statistical

comparison between groups was carried out using the Mann-Whitney U test (MWU) in IBM SPSS version 22.

3.6 Local field potential recording analysis

Local field potentials were analyzed by using a customized Matlab script (The MathWorks Inc., 2013a). For each recorded slice, the power spectral density was calculated using Welch's method, estimating the signal power at different frequencies. The spectral density estimation was computed for every 10 s using a Hamming window (8192 samples in length). Recordings were analyzed for the interval of 2000 to 7400 s. The beginning of this 90-minute interval (2000 s) was selected since control slices displayed stable gamma oscillations 1000 s after initial exposure to Cch. The recorded slices were classified based on the electrophysiological activity as follows: 1) continuous gamma oscillations throughout the 90-minute interval, 2) discontinuous gamma oscillations (partial gammas), or 3) no gamma-band oscillatory activity (non-responders). The median of the peak frequency and power for the interval length was calculated only for the slices displaying continuous gamma oscillations. Comparison between the medians of the different groups was carried out using the Kruskal-Wallis independent sample tests for three-group comparison, as well as the Mann-Whitney U test for two-group comparison. The number of slices displaying each of the three types of electrophysiological activity described above was compared between conditions using a two-tailed Fisher's exact test and presented as a percentage.

3.7 Fluorescent GSH labelling and quantification

Slices were incubated for 30 minutes with 50 µM monochlorobimane (mBCI) by adding it to the culturing medium (serum-free). This cell-permeable probe is not fluorescent until it forms an adduct with GSH, allowing fluorescent cell identification and spectrophotometrical quantification of GSH content. In situ imaging of the mCBI staining was performed on slices at DIV10 and 15 using a spinning disk microscope (see Section 3.5). Slices were transferred to a recording chamber perfused with warmed and gassed aCSF and imaged in the CA3 hippocampal region. For total-tissue GSH quantification, slices incubated with mCBI were detached from the membrane inserts, collected, and frozen in liquid nitrogen. Spectrophotometrical fluorescence quantification of mCBI from slice lysates and protein quantification (BSA assay) followed (not performed by the author –see Hasam-Henderson et al., 2018). Each experiment and condition included 9 to 18 slices obtained from 3-4 rats, which

were pooled together in order to attain sufficient protein for later quantification and to attenuate inter-slice variability.

3.8 Oxidized protein quantification

In order to investigate the levels of protein oxidation in control and treated slices the oxyblot assay (OxyBlot Protein Oxidation Detection Kit, Merck Chemicals) was used. This assay evaluates the protein oxidative modification by labelling the carbonyl groups. For each experiment 7 µg of protein homogenate, obtained from 9-18 slices (3-4 rats), was analyzed according to the manufacturer's protocol, followed by a staining densitometric analysis in the range of 40 and 130 kDa (QuantityOne Software). For each experiment, 3 to 6 oxyblots were carried out, where the means were used as statistical analysis (One-way Anova test, Bonferroni correction method for multiple comparisons) (70). The protein quantification was not performed by the author –see Hasam-Henderson *et al*., 2018 (68).

3.9 Recultivating protocol

Organotypic slice cultures were cut out from the culture insert membrane and were transported from the incubator to a spinning disk confocal microscope from DIV4 to 10 for repeated imaging sessions. Slices were submerged in pre-warmed sterile MEM and consecutive images covering the whole hippocampus (15-20 focal planes at 1µm distance) were acquired with a 20x water immersion objective. After the imaging sessions, the extra MEM was removed, membrane patches carrying the slices were placed on fresh culture insert and returned to the incubator for further cultivation. The acquired images were arranged into hippocampal panorama pictures (Image acquisition and analysis section). At DIV15, slices were fixed and processed for PV immunolabelling (see Section 3.4). Panorama reconstructions were acquired using multiphoton microscopy (see Section 3.5).

4. Results

4.1 *In vitro* development of PV expression and gamma oscillations in hippocampal slice cultures

PV expression and gamma oscillations were characterized in slice cultures at different culturing stages. PV expression markedly increased from 1% of all interneurons at the time of slice preparation (DIV0, P6-7, n=6) to 4% at DIV3 (n=15), and then to 17% by DIV10 (n=13). No further increase was detected by DIV15 (16.5%, n=20). Acute slices prepared from rats at P21-22 (n=7), corresponding in age to DIV15 slices, reflected a similar ratio of PV+ interneurons

(16.4%), suggesting that the *in vitro* development of PV expression is comparable to that observed *in vivo*.

Local field potential recordings of gamma oscillations acquired from the CA3 region of slices at DIV3 and 10 showed an increase in peak frequency and power in relation with the time spent in culture (frequency: 32 Hz to 40 Hz, $p=5.62^{-10}$; power: 1.3 μV^2 to 4.9 μV^2, $p=1.5^{-5}$, n=47 and 38, MWU). No further significant increase was observed between DIV10 and 15 (frequency: 40 Hz and 41 Hz, p=0.4536; power: 4.9 μV^2, 3.1 μV^2, p=0.4022, n=38 and 10, MWU). Cultures aged over DIV10 were more susceptible to develop fragmented gamma oscillations which intermingled with recurrent epileptiform discharges after > ~60 min of Cch exposure. The percentage of responder slices presenting continuous and uninterrupted gamma oscillations during the 90-min recording interval gradually dropped from 51% at DIV3 to 17% at DIV15. Therefore, we excluded this late culturing stage from our pharmacological study.

The developmental changes in the gamma oscillation properties followed the time course of the electrophysiological maturation of non-adapting fast-spiking interneurons (putative PV+ basket cells). Whole-cell patch clamp recordings of these cells, performed in slices from DIV2 to 17, displayed a negative correlation between DIV and membrane resistance ($p < 0.01$, two-tailed Spearman correlations, ρ:-0.485) and action potential (AP)-half-width (ρ: -0.428), while a positive correlation was observed for membrane capacitance (ρ:0.368) and maximum AP-frequency (ρ: 0.657). The maximum AP-frequency and AP-half-width reached a plateau by DIV 9 (see Hasam-Henderson *et al.*, 2018 (68), the author did not perform these experiments). Simultaneous to the increase in membrane capacitance and decrease in membrane resistance of non-adapting fast-spiking interneurons between DIV3 and 10, an increase in interneuron dendritic and axonal arborization was detected. Consequently, a protocol that allowed the tracing of single interneurons during the time course of the *in vitro* cultivation was established. This was achieved by imaging a given slice at different culturing time points (DIV4, 10, and 15), which was returned to the incubator between microscopy sessions (Figure 1). Using this method it was possible to confirm that the time-dependent increase in the PV+/YFP ratio results from the rise of PV expression, as PV+ cells at DIV15 could be traced back to DIV4, the point at which the PV+/YFP ratio was smaller. Furthermore, combining this method with whole-cell patch clamp recordings and neurobiotin labelling, could facilitate the study of anatomical and structural changes occurring to single interneurons during *in vitro* cultivation in control and treated conditions.

To further characterize the PV+ interneuron maturation, preliminary microscopy assessments of DIV3 and DIV10 control slices showed that the perineuronal nets (PNNs), typically

enwrapping PV+ interneurons, are preserved and develop *in vitro* (Figure 2). Altogether, these results confirmed the ongoing maturation of PV+ interneurons and of the hippocampal network in culture, which, in this model, reached a plateau by DIV10.

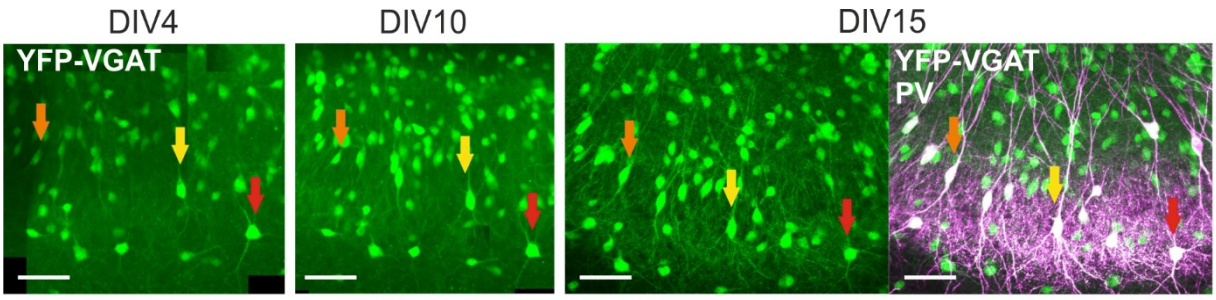

Figure 1. Single-interneuron tracing at different culturing time points. Image close-ups to YFP-VGAT interneurons (green) in the CA3 region of a slice (*ex vivo*) at DIV4 and DIV10 and after fixation and PV immunolabelling (magenta) at DIV15 (Scale bar 30 µm).

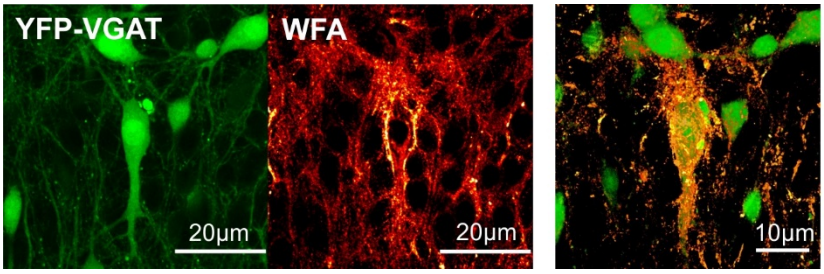

Figure 2. PNNs in slice cultures. Labelling of a DIV10 slice culture with the *Wisteria Floribunda* agglutinin (red) revealed tight PNNs surrounding individual VGAT-YFP interneurons (green).

4.2 NMDAR inhibition reduced the frequency of gamma oscillations before decreasing PV expression

NMDAR inhibition induced by APV exposure resulted in sustained decrease in the peak frequency of gamma oscillations at both developmental time points (DIV3: Control 31.7 Hz, n=47; APV 27.2 Hz, n=14, p=0.0031; DIV10: Control 39.7 Hz, n=38; APV 36.6 Hz, n=14, p=0.0254, MWU). This frequency drop was not reflected in the ability of the slices to develop and sustain continuous gamma oscillations, which were comparable to the control conditions. Interestingly, changes in the PV expression were not simultaneous to the alterations in gamma-band activity and a significant decrease could be observed only at DIV10 (control 16.8%, n=13; APV 13.1%, n=10, p=0.0256, MWU). These results suggest that changes in network gamma-band activity can be upstream to (or independent of) the loss of the PV phenotype.

4.3 Induction of oxidative stress temporarily increases the power of gamma oscillations while simultaneously decreasing PV expression

In contrast to NMDAR inhibition, oxidative stress induced by partial GSH and Trx inhibition did not change the peak frequency of gamma oscillations, but instead resulted in an acute (DIV3) increase in the peak power (control 1.3 μV^2, n= 47; BSO/Au 2.39 μV^2, n= 35, p=0.0273, MWU) which was not maintained up to DIV10. At this late culturing stage, the number of responder slices displaying continuous gamma oscillations almost doubled with respect to the control group (control 38%, n=100, BSO/Au 70%, n=56, p=0.0094, two-tailed Fisher's exact test). Assessment of PV expression showed that PV loss (control 4.3%, n=15; BSO/Au 3%, n= 12, p=0.010, MWU) concurred with the transient increase in power. Although the percentage of PV+ interneurons was similar by DIV10 to that of the control tissue, an apparent decrease in the number of interneurons led to a significant increase in the ratio of YFP/PV+ interneurons. In order investigate the transient effect of oxidative stress on the gamma oscillations, the BSO/Au treatment was applied in slice cultures at a later developmental stage (from DIV8 to 10, same exposure duration as from DIV1 to 3). The peak frequency and power of gamma oscillations did not differ from those observed in the control group, suggesting that the electrophysiological effects of oxidative stress might depend on the neuronal developmental stage, i.e., an already mature network is less susceptible to oxidative stress.

4.4 Increased synaptic transmission transiently decreases the frequency of gamma oscillations without affecting PV expression

Enhanced synaptic transmission evoked by exposure to 4AP did not alter the peak power of gamma oscillations but lead to a transient (DIV3) decrease in the peak frequency (control 31.7 Hz, n= 47; 4AP 25.6 Hz, n=15, p=0.0054, MWU), returning to control values by DIV10. Similar to that observed in the oxidative stress treatment at DIV10, slices displayed a higher propensity to maintain gamma oscillations doubling that of the control group (control 38%, n=100, 4AP 80%, n=25, p< 0.001, two-tailed Fisher's exact test). Interestingly, the augmented responder rates were not accompanied by a reduction in PV expression, but rather an increase in the interneurons' survival was observed at both DIV3 and 10 (DIV3 control 111.8, n=15; 4AP 163.8, n=10, p=0.0229; DIV10 control 80.5, n=13; 4AP 111.4, n=11, p=0.0050, number of interneurons per image stack, MWU). These results are in line with the findings obtained in cultures exposed to NMDAR inhibition, where the alterations in the gamma-band activity did not coincide with the changes in PV expression. Additionally, in this slice culture model,

enhancing synaptic activity not only promoted interneuron survival, but also the ability of the network to sustain long periods of gamma oscillations.

4.5 Total GSH content decreases after induction of oxidative stress but remains unchanged after NMDAR inhibition and enhanced synaptic transmission

The GSH and Trx antioxidant systems were partially blocked with the aim of inducing subliminal oxidative stress, which would not affect the viability of the slices. This was accomplished by exposure to BSO and Au (1 µM and 1 µM, higher doses of BSO were deleterious), resulting in a total tissue GSH decrease of 45% and 28% at DIV3 and 10 respectively, with respect to control (DIV3 n=5 and 13 rats, $p<0.001$; DIV10 n=4 and 12 rats, $p=0.002$, ANOVA, Bonferroni post-hoc). Altogether, these experiments demonstrated that a GSH reduction in the range of 28-45% is enough to disturb the hippocampal network and PV+ interneuron function, which is in line with *in vivo* findings showing behavioral disturbances induced by BSO exposure in young animals (37). On the contrary, neither NMDAR inhibition nor enhanced synaptic transmission affected the GSH content, implying that in this experimental setting, the capacity of this antioxidant system was independent from NMDAR function and increased synaptic activity. Microscopic assessment of the cellular distribution of the mBCI staining indicated that glial cells present higher GSH concentration compared to the YFP+ interneuron population.

4.6 Levels of protein oxidation increase after first exposure to all treatments

In order to assess whether the different treatments could increase oxidative stress independently from the GSH antioxidant system, protein oxidation levels were measured using oxyblot assays. This set of experiments showed that at DIV3 all treatments increased protein oxidation (control 100%, n=4; APV 126.8 ± 11.5 %, n= 4, $p=0.028$; BSO/Au 141.2 ± 4 %, n= 4, $p=0.002$, 4AP 144.1 ± 19.1%, n=3, $p<0.001$, mean ± SD, ANOVA, Bonferroni post-hoc), however by DIV10 this increase lost significance. Analysis of the course of protein oxidation in control slices at different culturing time points (DIV0, 4, 7, 10) reflected a progressive increase in oxidation peaking at DIV7 and decreasing by DIV10. This model-intrinsic recovery in late culturing stages hints to the development of adaptive antioxidant responses, which could help slices to overcome the oxidative stress exerted by the treatments.

4.7 Combined exposure to oxidative stress and enhanced synaptic transmission alters the frequency of gamma oscillations and increases responder rates

The effects of simultaneous exposure to 4AP and BSO/Au on gamma oscillations differed from those of the isolated treatments. This combined treatment initially (DIV3) decreased the peak frequency (control 31.7 Hz, n= 47, 4AP/BSO/Au 27.5 Hz, n=17, p=0.0015, MWU), similar to 4AP, but unlike the BSO/Au treatment. At DIV10, the decrease was transformed into a frequency rise surpassing control levels (control 39.7 Hz, n=38, 4AP/BSO/Au 47.9 Hz, n=12, p=0.0007, MWU). Similarly to the findings in the BSO/Au or 4AP treatments, the number of slices displaying continuous gamma oscillations was higher than in control groups at both DIV3 and 10 (DIV3: 51% vs 74%, n= 93 and 23, $p<0.01$; DIV10 38% vs 67%, n=100 and 18, $p<0.01$, two-tailed Fisher's exact test). Quantification of the total GSH content showed that in this combined treatment the GSH concentration decreased significantly (DIV3 $p<0.001$, DIV10 $p=0.001$), similar to that of the oxidative stress treatment alone. These findings point to a complex synergistic effect in which the contribution of the isolated treatments is no longer unraveled.

4.8 Lower levels of oxidative stress increase gamma oscillation responder rates without affecting the frequency or power

To investigate if even milder oxidative stress would still interfere with the gamma-band oscillatory activity, lower concentrations of BSO and Au were used (0.5 µM and 0.5 µM). A preliminary spectrophotometric quantification performed in slices at DIV3 pointed to a 23% reduction in total GSH content, compared to the 45% observed in the higher-dose treatment (1 µM and 1µM). This treatment did not alter the peak frequency or power of gamma oscillations. However, by DIV10, similarly to the case of 1µM BSO/Au, an increase in the number of slices displaying continuous gamma oscillations was observed with respect to the control group (38% vs 68%, n=100 and 25, $p<0.05$, two-tailed Fisher's exact test). This suggests that even mild oxidative stress during *in vitro* neuronal development has a strong impact on the network's properties, despite the unchanged frequency and power.

5. Discussion

In spite of the unclear etiology, accumulating evidence suggests that both NMDAR hypofunction and oxidative stress during neuronal maturation contribute to the manifestation of schizophrenia (3, 25, 29). The aim of this study was to disentangle the effects that NMDAR hypofunction and oxidative stress would exert on a developing neuronal network. Alterations

of the gamma-band activity and loss of interneuron PV phenotype are thought to be causally linked to schizophrenia symptoms (7), motivating my investigation of these parameters. In order to carry out this study, a model based on hippocampal slice cultures was established, allowing the assessment of different postnatal neurodevelopmental stages by combining pharmacological treatments, immunocytochemistry and electrophysiological techniques.

In order to exclude culture-dependent modifications, which could interfere with the interpretation of the study, we first validated the model by characterizing the *in vitro* development of gamma oscillations and by comparing the maturation of PV expression with age-matched acute slices. PV expression and gamma oscillation properties developed similarly to *in vivo* conditions up to DIV10 (68, Hasam-Henderson, *et al.*, 2018; Klemz *et al*., in preparation). However, slices cultured for longer periods (DIV15) displayed an increased propensity to develop epileptiform activity during carbachol exposure, which could be explained by the axonal reorganization occurring in explanted cultures resulting from lack of external input and cell loss (61, 72). Although these changes were not assessed in this study, we have introduced a recultivating protocol that, combined with electrophysiological and labelling techniques, could offer a unique possibility to investigate anatomical modifications taking place at the level of individual interneurons during *in vitro* cultivation.

The second part of the study shows that both NMDAR inhibition and oxidative stress, induced by a partial blockade of the GSH and Trx antioxidant systems, differentially altered gamma oscillations and PV expression. NMDAR inhibition evoked an immediate (DIV3) and sustained (DIV10) decrease in the peak frequency while the loss of PV expression was only significant at DIV10. In line with these findings, previous studies have reported that repeated neonatal NMDAR antagonism (from P6 to 10), when compared to single exposure, progressively increased the loss of PV in cingulate cortex (73). This loss, accompanied by a decrease in the gamma oscillation power, was also observed in the hippocampus of rats exposed chronically to ketamine (74). Furthermore, consecutive blockade of NMDAR with MK-801 at similar developmental stages (from P5 to P14), led to decreased hippocampal PV and VGAT expression in adolescence (P35) and adulthood (P63) (75), while a single PCP dose at P7 was not enough to affect hippocampal PV expression (17). Regarding the contributions of NMDAR antagonism on hippocampal gamma oscillations, various effects ranging from decreased to increased frequency and power have been reported. This variability arises from differences across experimental and pharmacological regimes (76).

Although the mechanisms underlying the postnatal susceptibility of PV+ basket cells to NMDAR hypofunction are unclear, the late development of these interneurons is believed to be

critically involved (29, 77, 78, 79). The maturation of PV+ basket cells is activity-dependent and programmed to occur postnatally (41, 42, 80), in the same period at which (first two postnatal weeks) NMDAR expression peaks (81) and changes in their subunit composition occur (82). NMDA-mediated excitatory transmission is strongly involved in synaptogenesis and pruning (77, 82, 83, 84, 85). Thus, during early postnatal development, NMDAR hypofunction could interfere with the maturation of the PV+ fast-spiking interneurons and disturb the network formation (86). In this experimental setting, this could underlie the sustained reduction in the peak frequency of gamma oscillations.

In contrast to NMDAR inhibition, oxidative stress induced by the partial blockade of the GSH and Trx systems elicited an acute and transient (DIV3) increase in the peak power of gamma oscillations, simultaneous to a reduction in PV expression. These results are in line with previous studies reporting loss of PV and GAD67 expression and impaired high-frequency neuronal synchrony elicited by perinatal redox dysregulation (15, 55). These alterations are suggested to reflect disturbances in the maturation of PV+ basket cells and aberrant neuronal wiring evoked by oxidative stress-mediated NMDAR hypofunction (55). Oxidative stress, including GSH deficiency, is known to decrease NMDAR activity via oxidation of their extracellular redox-sensitive sites (28, 38, 88). Since synaptic NMDAR activity is coupled to the transcriptional control of the GSH and Trx systems, the hypofunction of these receptors could lead to a weakened antioxidant defense (25, 54, 55, 56, 57).

In the current study, despite the continuity of the oxidative stress, the loss of PV and increased gamma power was not maintained up to DIV10, suggesting an adaptive response which could involve the up-regulation of compensatory antioxidant defenses under the control of the transcription factor Nrf2 (factor-erythroid 2-related factor 2). Oxidative stress is known to inhibit the degradation of this factor, thereby activating the antioxidant response element promoter and modulating mitochondrial ROS production and function (56, 57, 89, 90, 91). Although the PV expression and gamma power returned to control values by DIV10, slices exposed to sustained oxidative stress (even after a milder GSH/Trx inhibition) displayed longer and uninterrupted periods of gamma oscillations, compared to control slices. This reflects that, although the oxidative stress might be compensated, functional alterations of the network persisted.

Interestingly, in slices exposed to the same oxidative stress at a later developmental stage (DIV8 instead of DIV1), the gamma oscillation parameters were unchanged, pointing to a susceptibility window to redox-imbalance before the first two postnatal weeks (81, 86, 92). This coincides with the oxidative stress sensitivity described for immature PV+ basket cells during

early postnatal development (first two postnatal weeks) associated with the emerging PV expression, undeveloped PNNs and feebled antioxidant systems (71).

Contrasting with previous findings associating GSH transcription to NMDAR activity (54), in this experimental setting GSH levels were unchanged upon NMDAR blockade and enhanced synaptic activity. However, the methodological approach of assessing the total tissue GSH content might not reflect the small GSH variations in the interneurons, which could have a profound impact on the network. Although the measured GSH levels were unchanged, an increase in oxidative stress was detected at DIV3, as shown by the elevated levels of oxidized protein residues observed in all treatments. This might originate from a model-intrinsic tendency to oxidative stress (interface culture conditions at 20% pO_2 resulting in ~300mmHg at the slice surface), which might be exacerbated by the exposure to the different treatments before it is reversed by the activation of adaptive/compensatory antioxidant response (25, 54, 89, 91).

6. Concluding remarks

In conclusion, NMDAR inhibition and oxidative stress induced by a partial GSH and Trx depletion decreased PV expression and altered gamma oscillations, although in a differential manner. In fact, the resulting changes and their time course suggest that NMDAR inhibition and oxidative stress exert independent effects on the development of the hippocampal network. While both treatments initially induced oxidative stress, the loss of PV expression and altered gamma power were acute and only transient in GSH/Trx-depleted cultures, whereas in the presence of the NMDAR inhibitor the loss of PV developed gradually following the drop in the frequency of gamma oscillations. Remarkably, enhancing synaptic activity mimicked the acute effect of NMDAR inhibition on gamma oscillations and did not modify the PV expression. Thus, although changes in PV expression and in the gamma-band activity properties are common hallmarks in schizophrenia, our data indicates that they could represent independent components of the disease.

7. Outlook

The recovery of the transient PV loss and increased gamma oscillation power in cultures exposed to GSH and Trx depletion, as well as their increased ability to maintain gamma activity at DIV10, could result from the presence and protective role of PNNs. These nets protect PV+ interneurons against oxidative stress whereas their degradation can reactivate periods of network plasticity (93, 94). During this study, I produced preliminary data demonstrating that

PNNs are present and develop *in vitro*, however, the possible changes induced by oxidative stress remain to be investigated.

Dystrophic oligodendrocytes and disturbances in the myelination have been reported in tissue samples of schizophrenia patients (95) and nearly all myelinated GABAergic axons in the cortex are PV+ (96). Oxidative stress affecting oligodendrocytes during perinatal maturation could disturb the formation of myelin sheaths altering the function of PV+ interneurons and the gamma oscillations properties. In preliminary experiments, I have shown that oligodendrocytes are retained in hippocampal cultures, thereby enabling the study of oxidative stress-dependent alterations in myelination.

8. References

1. Galderisi, S., Mucci, A., Buchanan, R. W. & Arango, C. Negative symptoms of schizophrenia: new developments and unanswered research questions. The Lancet Psychiatry 5, 664–677 (2018).
2. Lewis, D. A., Curley, A. A., Glausier, J. R. & Volk, D. W. Cortical parvalbumin interneurons and cognitive dysfunction in schizophrenia. Trends in Neurosciences 35, 57–67 (2012).
3. Do, K. Q., Cabungcal, J. H., Frank, A., Steullet, P. & Cuenod, M. Redox dysregulation, neurodevelopment, and schizophrenia. Curr. Opin. Neurobiol. 19, 220–230 (2009).
4. Gandal, M. J., Edgar, J. C., Klook, K. & Siegel, S. J. Gamma synchrony: towards a translational biomarker for the treatment-resistant symptoms of schizophrenia. Neuropharmacology 62, 1504–1518 (2012).
5. Uhlhaas, P. J. & Singer, W. Oscillations and Neuronal Dynamics in Schizophrenia: The Search for Basic Symptoms and Translational Opportunities. Biological Psychiatry 77, 1001–1009 (2015).
6. Reilly, T. J., Nottage, J.F., Studerus, E., Rutigliano, G., Micheli, A.I.D., Fusar-Poli, P., and McGuire, P. Gamma band oscillations in the early phase of psychosis: A systematic review. Neurosci Biobehav Rev 90, 381–399 (2018).
7. McNally, J. M. & McCarley, R. W. Gamma band oscillations: a key to understanding schizophrenia symptoms and neural circuit abnormalities. Current Opinion in Psychiatry 29, 202–210 (2016).
8. Volman, V., Behrens, M. M. & Sejnowski, T. J. Downregulation of parvalbumin at cortical GABA synapses reduces network gamma oscillatory activity. J. Neurosci. 31, 18137–18148 (2011).
9. Gonzalez-Burgos, G., Fish, K. N. & Lewis, D. A. GABA Neuron Alterations, Cortical Circuit Dysfunction and Cognitive Deficits in Schizophrenia. Neural Plasticity 2011, 1–24 (2011).
10. Fisahn, A., Pike, F. G., Buhl, E. H. & Paulsen, O. Cholinergic induction of network oscillations at 40 Hz in the hippocampus *in vitro*. Nature 394, 186–189 (1998).
11. Bartos, M., Vida, I., Frotscher, M., Meyer, A., Monyer, H., Geiger, J.R.P., and Jonas, P. Fast synaptic inhibition promotes synchronized gamma oscillations in hippocampal interneuron networks. Proc. Natl. Acad. Sci. U.S.A. 99, 13222–13227 (2002).
12. Bartos, M., Vida, I. & Jonas, P. Synaptic mechanisms of synchronized gamma oscillations in inhibitory interneuron networks. Nat. Rev. Neurosci. 8, 45–56 (2007).
13. Hájos, N., Pálhalmi, J., Mann, E.O., Németh, B., Paulsen, O., and Freund, T.F. Spike timing of distinct types of GABAergic interneuron during hippocampal gamma oscillations *in vitro*. J. Neurosci. 24, 9127–9137 (2004).
14. Furth, K. E., Mastwal, S., Wang, K. H., Buonanno, A. & Vullhorst, D. Dopamine, cognitive function, and gamma oscillations: role of D4 receptors. Front Cell Neurosci 7, 102 (2013).
15. Uhlhaas, P. J. & Singer, W. Abnormal neural oscillations and synchrony in schizophrenia. Nature Reviews Neuroscience 11, 100–113 (2010).
16. Manseau, F., Marinelli, S., Méndez, P., Schwaller, B., Prince, D.A., Huguenard, J.R., and Bacci, A. Desynchronization of Neocortical Networks by Asynchronous Release of GABA at Autaptic and Synaptic Contacts from Fast-Spiking Interneurons. PLoS Biology 8, e1000492 (2010).
17. Wang, C. Z., Yang, S. F., Xia, Y. & Johnson, K. M. Postnatal phencyclidine administration selectively reduces adult cortical parvalbumin-containing interneurons. Neuropsychopharmacology 33, 2442–2455 (2008).
18. Wang, A. Y., Lohmann, K.M., Yang, C.K., Zimmerman, E.I., Pantazopoulos, H., Herring, N., Berretta, S., Heckers, S., and Konradi, C. Bipolar disorder type 1 and schizophrenia are accompanied by decreased density of parvalbumin- and somatostatin-positive interneurons in the parahippocampal region. Acta Neuropathologica 122, 615–626 (2011).
19. Zhang, Z., Sun, J. & Reynolds, G. P. A selective reduction in the relative density of parvalbumin-immunoreactive neurons in the hippocampus in schizophrenia patients. Chin. Med. J. 115, 819–823 (2002).
20. Krystal, J. H., Karper, L.P., Seibyl, J.P., Freeman, G.K., Delaney, R., Bremner, J.D., Heninger, G.R., Bowers, M.B., and Charney, D.S. Subanesthetic effects of the noncompetitive NMDA antagonist, ketamine, in humans. Psychotomimetic, perceptual, cognitive, and neuroendocrine responses. Arch. Gen. Psychiatry 51, 199–214 (1994).
21. Coyle, J. T. The glutamatergic dysfunction hypothesis for schizophrenia. Harv Rev Psychiatry 3, 241–253 (1996).
22. Rivolta, D., Heidegger, T., Scheller, B., Sauer, A., Schaum, M., Birkner, K., Singer, W., Wibral, M. and Uhlhaas, P.J. Ketamine Dysregulates the Amplitude and Connectivity of High-Frequency Oscillations in Cortical–Subcortical Networks in Humans: Evidence From Resting-State Magnetoencephalography-Recordings. Schizophrenia Bulletin 41, 1105–1114 (2015).
23. Catts, V. S., Lai, Y. L., Weickert, C. S., Weickert, T. W. & Catts, S. V. A quantitative review of the postmortem evidence for decreased cortical N-methyl-d-aspartate receptor expression levels in schizophrenia: How can we link molecular abnormalities to mismatch negativity deficits? Biological Psychology 116, 57–67 (2016).
24. Schizophrenia Working Group of the Psychiatric Genomics Consortium. Biological insights from 108 schizophrenia-associated genetic loci. Nature 511, 421–427 (2014).
25. Hardingham, G. E. & Do, K. Q. Linking early-life NMDAR hypofunction and oxidative stress in schizophrenia pathogenesis. Nat. Rev. Neurosci. 17, 125–134 (2016).
26. Kinney, J. W., Davis, C.N., Tabarean, I., Conti, B., Bartfai, T., and Behrens, M.M. A specific role for NR2A-containing NMDA receptors in the maintenance of parvalbumin and GAD67 immunoreactivity in cultured interneurons. J. Neurosci. 26, 1604–1615 (2006).
27. Belforte, J. E., Zsiros, V., Sklar, E.R., Jiang, Z., Yu, G., Li, Y., Quinlan, E.M., and Nakazawa, K. Postnatal NMDA receptor ablation in corticolimbic interneurons confers schizophrenia-like phenotypes. Nat. Neurosci. 13, 76–83 (2010).
28. Cohen, S. M., Tsien, R. W., Goff, D. C. & Halassa, M. M. The impact of NMDA receptor hypofunction on GABAergic neurons in the pathophysiology of schizophrenia. Schizophr. Res. 167, 98–107 (2015).
29. Nakazawa, K., Jeevakumar, V. & Nakao, K. Spatial and temporal boundaries of NMDA receptor hypofunction leading to schizophrenia. npj Schizophrenia 3, (2017).
30. Korotkova, T., Fuchs, E. C., Ponomarenko, A., von Engelhardt, J. & Monyer, H. NMDA receptor ablation on parvalbumin-positive interneurons impairs hippocampal synchrony, spatial representations, and working memory. Neuron 68, 557–569 (2010).

31. Do, K. Q., Trabesinger, A.H., Kirsten-Krüger, M., Lauer, C.J., Dydak, U., Hell, D., Holsboer, F., Boesiger, P., and Cuénod, M. Schizophrenia: glutathione deficit in cerebrospinal fluid and prefrontal cortex *in vivo*. Eur. J. Neurosci. 12, 3721–3728 (2000).
32. Nucifora, L. G., Tanaka, T., Hayes, L.N., Kim, M., Lee, B.J., Matsuda, T., Nucifora, F.C., Sedlak, T., Mojtabai, R., Eaton, W., Sawa, A. Reduction of plasma glutathione in psychosis associated with schizophrenia and bipolar disorder in translational psychiatry. Transl Psychiatry 7, e1215 (2017).
33. Poels, E. M. P., Kegeles, L.S., Kantrowitz, J.T., Javitt, D.C., Lieberman, J.A., Abi-Dargham, A., and Girgis, R.R. Glutamatergic abnormalities in schizophrenia: a review of proton MRS findings. Schizophr. Res. 152, 325–332 (2014).
34. Berk, M., Copolov, D., Dean, O., Lu, K., Jeavons, S., Schapkaitz, I., Anderson-Hunt, M., Judd, F., Katz, F., Katz, P., Ording-Jespersen, S., Little, J., Conus, P., Cuenod, M., Do, K.Q., Bush, A.I. N-acetyl cysteine as a glutathione precursor for schizophrenia--a double-blind, randomized, placebo-controlled trial. Biol. Psychiatry 64, 361–368 (2008).
35. Yolland, C. O. B., Phillipou, A., Castle, D.J., Neill, E., Hughes, M.E., Galletly, C., Smith, Z.M., Francis, P.S., Dean, O.M., Sarris, J., Siskind, D., Harris, A.W.F., Rossell, S.L. Improvement of cognitive function in schizophrenia with N -acetylcysteine: A theoretical review. Nutritional Neuroscience 1–10 (2018).
36. das Neves Duarte, J. M., Kulak, A., Gholam-Razaee, M.M., Cuenod, M., Gruetter, R., and Do K.Q. N-Acetylcysteine Normalizes Neurochemical Changes in the Glutathione-Deficient Schizophrenia Mouse Model During Development. Biological Psychiatry 71, 1006–1014 (2012).
37. Steullet, P., Cabungcal, J.-H., Kulak, A., Kraftsik, R., Chen, Y., Dalton, T.P., Cuenod, M., and Do, K.Q. Redox dysregulation affects the ventral but not dorsal hippocampus: impairment of parvalbumin neurons, gamma oscillations, and related behaviors. J. Neurosci. 30, 2547–2558 (2010).
38. Steullet, P., Neijt, H. C., Cuénod, M. & Do, K. Q. Synaptic plasticity impairment and hypofunction of NMDA receptors induced by glutathione deficit: relevance to schizophrenia. Neuroscience 137, 807–819 (2006).
39. Behrens, M. M., Ali, S.S., Dao, D.N., Lucero, J., Shekhtman, G., Quick, K.L., and Dugan, L.L. Ketamine-induced loss of phenotype of fast-spiking interneurons is mediated by NADPH-oxidase. Science 318, 1645–1647 (2007).
40. Wang, X., Pinto-Duarte, A., Sejnowski, T. J. & Behrens, M. M. How Nox2-Containing NADPH Oxidase Affects Cortical Circuits in the NMDA Receptor Antagonist Model of Schizophrenia. Antioxidants & Redox Signaling 18, 1444–1462 (2013).
41. Doischer, D., Aurel Hosp, J., Yanagawa, Y., Obata, K., Jonas, P., Vida, I., and Bartos, M. Postnatal Differentiation of Basket Cells from Slow to Fast Signaling Devices. Journal of Neuroscience 28, 12956–12968 (2008).
42. de Lecea, L., del Río, J. A. & Soriano, E. Developmental expression of parvalbumin mRNA in the cerebral cortex and hippocampus of the rat. Brain Res. Mol. Brain Res. 32, 1–13 (1995).
43. Du, J., Zhang, L., Weiser, M., Rudy, B. & McBain, C. J. Developmental expression and functional characterization of the potassium-channel subunit Kv3.1b in parvalbumin-containing interneurons of the rat hippocampus. J. Neurosci. 16, 506–518 (1996).
44. Tansey, E. P., Chow, A., Rudy, B. & McBain, C. J. Developmental expression of potassium-channel subunit Kv3.2 within subpopulations of mouse hippocampal inhibitory interneurons. Hippocampus 12, 137–148 (2002).
45. Permyakov, S. E., Kazakov, A. S., Avkhacheva, N. V. & Permyakov, E. A. Parvalbumin as a metal-dependent antioxidant. Cell Calcium 55, 261–268 (2014).
46. Hensch, T. K. Controlling the critical period. Neurosci. Res. 47, 17–22 (2003).
47. Cabungcal, J.-H., Steullet, P., Morishita, H., Kraftsik, R., Cuenod, M., Hensch, T.K., and Do, K.Q. Perineuronal nets protect fast-spiking interneurons against oxidative stress. Proc. Natl. Acad. Sci. U.S.A. 110, 9130–9135 (2013).
48. Mauney, S. A., Athanas, K.M., Pantazopoulos, H., Shaskan, N., Passeri, E., Berretta, S., and Woo, T.-U.W. Developmental pattern of perineuronal nets in the human prefrontal cortex and their deficit in schizophrenia. Biol. Psychiatry 74, 427–435 (2013).
49. Enwright, J. F., Sanapala, S., Foglio, A., Berry, R., Fish, K.N., and Lewis, D.A. Reduced Labeling of Parvalbumin Neurons and Perineuronal Nets in the Dorsolateral Prefrontal Cortex of Subjects with Schizophrenia. Neuropsychopharmacology 41, 2206–2214 (2016).
50. Berretta, S., Pantazopoulos, H., Markota, M., Brown, C. & Batzianouli, E. T. Losing the sugar coating: Potential impact of perineuronal net abnormalities on interneurons in schizophrenia. Schizophrenia Research 167, 18–27 (2015).
51. Hasenstaub, A., Otte, S., Callaway, E. & Sejnowski, T. J. Metabolic cost as a unifying principle governing neuronal biophysics. Proceedings of the National Academy of Sciences 107, 12329–12334 (2010).
52. Hu, H., Roth, F. C., Vandael, D. & Jonas, P. Complementary Tuning of Na + and K + Channel Gating Underlies Fast and Energy-Efficient Action Potentials in GABAergic Interneuron Axons. Neuron 98, 156-165.e6 (2018).
53. Gulyás, A. I., Buzsáki, G., Freund, T. F. & Hirase, H. Populations of hippocampal inhibitory neurons express different levels of cytochrome c. European Journal of Neuroscience 23, 2581–2594 (2006).
54. Baxter, P. S., Bell, K.F.S., Hasel, P., Kaindl, A.M., Fricker, M., Thomson, D., Cregan, S.P., Gillingwater, T.H., and Hardingham, G.E. Synaptic NMDA receptor activity is coupled to the transcriptional control of the glutathione system. Nat Commun 6, 6761 (2015).
55. Steullet, P., Cabungcal, J.-H., Coyle, J., Didriksen, M., Gill, K., Grace, A.A., Hensch, T.K., LaMantia, A.-S., Lindemann, L., Maynard, T.M., Meyer, U., Morishita, H., O'Donnell, P., Puhl, M., Cuenod, M., Do, K.Q. Oxidative stress-driven parvalbumin interneuron impairment as a common mechanism in models of schizophrenia. Molecular Psychiatry 22, 936–943 (2017).
56. Papadia, S., Soriano, F.X., Léveillé, F., Martel, M.-A., Dakin, K.A., Hansen, H.H., Kaindl, A., Sifringer, M., Fowler, J., Stefovska, V., Mckenzie, G., Craigon, M., Corriveau, R., Ghazal, P., Horsburgh, K., Yankner, B.A., Wyllie, D.J.A., Ikonomidou, C., Hardingham, G.E. Synaptic NMDA receptor activity boosts intrinsic antioxidant defenses. Nature Neuroscience 11, 476–487 (2008).
57. Bell, K. F. S. & Hardingham, G. E. The influence of synaptic activity on neuronal health. Curr. Opin. Neurobiol. 21, 299–305 (2011).
58. Behrens, M. M. & Sejnowski, T. J. Does schizophrenia arise from oxidative dysregulation of parvalbumin-interneurons in the developing cortex? Neuropharmacology 57, 193–200 (2009).

59. Stoppini, L., Buchs, P. A. & Muller, D. A simple method for organotypic cultures of nervous tissue. J. Neurosci. Methods 37, 173–182 (1991).
60. Uematsu, M., Hirai, Y., Karube, F., Ebihara, S., Kato, M., Abe, K., Obata, K., Yoshida, S., Hirabayashi, M., Yanagawa, Y., Kawaguchi, Y. Quantitative chemical composition of cortical GABAergic neurons revealed in transgenic venus-expressing rats. Cereb. Cortex 18, 315–330 (2008).
61. Gutiérrez, R. & Heinemann, U. Synaptic reorganization in explanted cultures of rat hippocampus. Brain Res. 815, 304–316 (1999).
62. Heinemann, U., Buchheim, K., Gabriel, S., Kann, O., Kovacs, R., and Schuchmann, S. Cell death and metabolic activity during epileptiform discharges and status epilepticus in the hippocampus. Progress in Brain Research 135, 197–210 (2002).
63. Kovacs, R., Schuchmann, S., Gabriel, S., Kardos, J. & Heinemann, U. Ca2+ signalling and changes of mitochondrial function during low-Mg2+-induced epileptiform activity in organotypic hippocampal slice cultures. Eur. J. Neurosci. 13, 1311–1319 (2001).
64. Kovács, R., Schuchmann, S., Gabriel, S., Kann, O., Kardos, J., and Heinemann, U. Free radical-mediated cell damage after experimental status epilepticus in hippocampal slice cultures. J. Neurophysiol. 88, 2909–2918 (2002).
65. Kovacs, R., Rabanus, A., Otahal, J., Patzak, A., Kardos, J., Albus, K., Heinemann, U., and Kann, O. Endogenous Nitric Oxide Is a Key Promoting Factor for Initiation of Seizure-Like Events in Hippocampal and Entorhinal Cortex Slices. Journal of Neuroscience 29, 8565–8577 (2009).
66. Mandal, P. K., Seiler, A., Perisic, T., Kölle, P., Banjac Canak, A., Förster, H., Weiss, N., Kremmer, E., Lieberman, M.W., Bannai, S., Kuhlencordt, P., Sato, H., Bornkamm, G.W., Conrad, M. System x c − and Thioredoxin Reductase 1 Cooperatively Rescue Glutathione Deficiency. Journal of Biological Chemistry 285, 22244–22253 (2010).
67. Ruszkiewicz, J. & Albrecht, J. Changes of the Thioredoxin System, Glutathione Peroxidase Activity and Total Antioxidant Capacity in Rat Brain Cortex During Acute Liver Failure: Modulation by l-histidine. Neurochemical Research 40, 293–300 (2015).
68. Hasam-Henderson, L. A., Gotti, G.C., Mishto, M., Klisch, C., Gerevich, Z., Geiger, J.R.P., and Kovács, R. NMDA-receptor inhibition and oxidative stress during hippocampal maturation differentially alter parvalbumin expression and gamma-band activity. Scientific Reports 8, (2018).
69. Preibisch, S., Saalfeld, S. & Tomancak, P. Globally optimal stitching of tiled 3D microscopic image acquisitions. Bioinformatics 25, 1463–1465 (2009).
70. Mishto, M., Raza, M.L., de Biase, D., Ravizza, T., Vasuri, F., Martucci, M., Keller, C., Bellavista, E., Buchholz, T.J., Kloetzel, P.M., Pession, A., Vezzani, A., Heinemann, U. The immunoproteasome α5i subunit is a key contributor to ictogenesis in a rat model of chronic epilepsy. Brain, Behavior, and Immunity 49, 188–196 (2015).
71. Do, K. Q., Cuenod, M. & Hensch, T. K. Targeting Oxidative Stress and Aberrant Critical Period Plasticity in the Developmental Trajectory to Schizophrenia. Schizophr Bull 41, 835–846 (2015).
72. Albus, K., Heinemann, U. & Kovács, R. Network activity in hippocampal slice cultures revealed by long-term *in vitro* recordings. J. Neurosci. Methods 217, 1–8 (2013).
73. Turner, C. P., DeBenedetto, D., Ware, E., Stowe, R., Lee, A., Swanson, J., Walburg, C., Lambert, A., Lyle, M., Desai, P., Liu, C. Postnatal exposure to MK801 induces selective changes in GAD67 or parvalbumin. Experimental Brain Research 201, 479–488 (2010).
74. Kittelberger, K., Hur, E. E., Sazegar, S., Keshavan, V. & Kocsis, B. Comparison of the effects of acute and chronic administration of ketamine on hippocampal oscillations: relevance for the NMDA receptor hypofunction model of schizophrenia. Brain Structure and Function 217, 395–409 (2012).
75. Li, J.-T., Zhao, Y.-Y., Wang, H.-L., Wang, X.-D., Su, Y.-A., and Si, T.-M. Long-term effects of neonatal exposure to MK-801 on recognition memory and excitatory–inhibitory balance in rat hippocampus. Neuroscience 308, 134–143 (2015).
76. Jadi, M. P., Behrens, M. M. & Sejnowski, T. J. Abnormal Gamma Oscillations in N-Methyl-D-Aspartate Receptor Hypofunction Models of Schizophrenia. Biological Psychiatry 79, 716–726 (2016).
77. du Bois, T. M. & Huang, X.-F. Early brain development disruption from NMDA receptor hypofunction: Relevance to schizophrenia. Brain Research Reviews 53, 260–270 (2007).
78. Lim, A. L., Taylor, D. A. & Malone, D. T. Consequences of early life MK-801 administration: Long-term behavioural effects and relevance to schizophrenia research. Behavioural Brain Research 227, 276–286 (2012).
79. Kjaerby, C., Hovelsø, N., Dalby, N. O. & Sotty, F. Phencyclidine administration during neurodevelopment alters network activity in prefrontal cortex and hippocampus in adult rats. J. Neurophysiol. 118, 1002–1011 (2017).
80. Gu, X., Zhou, L. & Lu, W. An NMDA Receptor-Dependent Mechanism Underlies Inhibitory Synapse Development. Cell Reports 14, 471–478 (2016).
81. Awobuluyi, M., Lipton, S. A. & Sucher, N. J. Translationally distinct populations of NMDA receptor subunit NR1 mRNA in the developing rat brain. J. Neurochem. 87, 1066–1075 (2003).
82. Gambrill, A. C. & Barria, A. NMDA receptor subunit composition controls synaptogenesis and synapse stabilization. Proceedings of the National Academy of Sciences 108, 5855–5860 (2011).
83. Lüthi, A., Schwyzer, L., Mateos, J. M., Gähwiler, B. H. & McKinney, R. A. NMDA receptor activation limits the number of synaptic connections during hippocampal development. Nature Neuroscience 4, 1102–1107 (2001).
84. Lau, C. G. & Zukin, R. S. NMDA receptor trafficking in synaptic plasticity and neuropsychiatric disorders. Nature Reviews Neuroscience 8, 413–426 (2007).
85. Haberny, K. A. Ontogeny of the N-Methyl-D-Aspartate (NMDA) Receptor System and Susceptibility to Neurotoxicity. Toxicological Sciences 68, 9–17 (2002).
86. Matta, J. A., Pelkey, K.A., Craig, M.T., Chittajallu, R., Jeffries, B.W., and McBain, C.J. Developmental origin dictates interneuron AMPA and NMDA receptor subunit composition and plasticity. Nature Neuroscience 16, 1032–1041 (2013).
87. Xi, D., Zhang, W., Wang, H.-X., Stradtman, G. G. & Gao, W.-J. Dizocilpine (MK-801) induces distinct changes of N-methyl-d-aspartic acid receptor subunits in parvalbumin-containing interneurons in young adult rat prefrontal cortex. The International Journal of Neuropsychopharmacology 12, 1395 (2009)

88. Köhr, G., Eckardt, S., Lüddens, H., Monyer, H. & Seeburg, P. H. NMDA receptor channels: subunit-specific potentiation by reducing agents. Neuron 12, 1031–1040 (1994).
89. Baxter, P. S. & Hardingham, G. E. Adaptive regulation of the brain's antioxidant defences by neurons and astrocytes. Free Radical Biology and Medicine 100, 147–152 (2016).
90. Kovac, S., Angelova, P.R., Holmström, K.M., Zhang, Y., Dinkova-Kostova, A.T., and Abramov, A.Y. Nrf2 regulates ROS production by mitochondria and NADPH oxidase. Biochimica et Biophysica Acta (BBA) - General Subjects 1850, 794–801 (2015).
91. Dinkova-Kostova, A. T. & Abramov, A. Y. The emerging role of Nrf2 in mitochondrial function. Free Radical Biology and Medicine 88, 179–188 (2015).
92. Contestabile, A. Roles of NMDA receptor activity and nitric oxide production in brain development. Brain Res. Brain Res. Rev. 32, 476–509 (2000).
93. Carulli, D., Pizzorusso, T., Kwok, J.C.F., Putignano, E., Poli, A., Forostyak, S., Andrews, M.R., Deepa, S.S., Glant, T.T., and Fawcett, J.W. Animals lacking link protein have attenuated perineuronal nets and persistent plasticity. Brain 133, 2331–2347 (2010).
94. Kim, S. Y., Senatorov, V.V., Morrissey, C.S., Lippmann, K., Vazquez, O., Milikovsky, D.Z., Gu, F., Parada, I., Prince, D.A., Becker, A.J., Heinemann, U., Friedman, A., Kaufer, D. TGFβ signaling is associated with changes in inflammatory gene expression and perineuronal net degradation around inhibitory neurons following various neurological insults. Scientific Reports 7, (2017).
95. Maas, D. A., Vallès, A. & Martens, G. J. M. Oxidative stress, prefrontal cortex hypomyelination and cognitive symptoms in schizophrenia. Translational Psychiatry 7, e1171 (2017).
96. Micheva, K. D., Wolman, D., Mensh, B.D., Pax, E., Buchanan, J., Smith, S.J., and Bock, D.D. A large fraction of neocortical myelin ensheathes axons of local inhibitory neurons. eLife 5, (2016).

Affidavit

I, Luisa Austin Hasam Henderson, certify under penalty of perjury by my own signature that I have submitted the thesis on the topic "*NMDA-receptor inhibition and oxidative stress during hippocampal maturation differentially alter parvalbumin expression and gamma-band activity*". I wrote this thesis independently and without assistance from third parties, I used no other aids than the listed sources and resources.

All points based literally or in spirit on publications or presentations of other authors are, as such, in proper citations (see "uniform requirements for manuscripts (URM)" the ICMJE www.icmje.org) indicated. The sections on methodology (in particular practical work, laboratory requirements, statistical processing) and results (in particular images, graphics and tables) correspond to the URM (s.o) and are answered by me. My contribution in the selected publication for this dissertation correspond to those that are specified in the following joint declaration with the responsible person and supervisor.

The importance of this affidavit and the criminal consequences of a false affidavit (section 156,161 of the Criminal Code) are known to me and I understand the rights and responsibilities stated therein.

_____ _____

Date Signature

Detailed declaration of contribution

Luisa Austin Hasam Henderson had the following share in the following publication:

Luisa A. Hasam-Henderson, Grace C. Gotti, Michele Mishto, Constantin Klisch, Zoltan Gerevich, Jörg R.P. Geiger, Richard Kovács. *NMDA-receptor inhibition and oxidative stress during hippocampal maturation differentially alter parvalbumin expression and gamma-band activity*. Scientific Reports, 2018.

Contribution in detail

Design of the experiments:

The experiments were designed by Kovács R. and Hasam-Henderson L.A.

Performance of the experiments and analysis:

Slice culture preparation and maintenance for all experiments was carried out by Hasam-Henderson L.A. Whole cell patch clamp recordings and analysis were performed by Gotti, G.C. (Figure 1d). Immunohistochemistry, microscopy and cell quantification were performed by Hasam-Henderson L.A. Gamma oscillation field potential recordings and analysis were performed by Hasam-Henderson L.A. and Klisch, C. Oxiblots assays and mCBI fluorescence analysis were performed by Mishto, M. (Figure 3a, b, c, d)

Manuscript writing and submission:

Manuscript writing and editing was performed by Hasam-Henderson L.A. and Kóvacs R. Manuscript figures were prepared by Hasam-Henderson L.A., with exception of Figure 1b and Figure 3. Contributions to the manuscript preparation were carried out by Geiger J. R. P. and Gerevich Z.

_____

Signature of doctoral candidate

Excerpt from the Journal Summary List (ISI Web of Knowledge)

Journal Data Filtered By: **Selected JCR Year: 2016** Selected Editions: SCIE,SSCI
Selected Categories: **"MULTIDISCIPLINARY SCIENCES"** Selected Category Scheme: WoS
Gesamtanzahl: 64 Journale

Rank	Full Journal Title	Total Cites	Journal Impact Factor	Eigenfactor Score
1	NATURE	671,254	40.137	1.433990
2	SCIENCE	606,635	37.205	1.159250
3	Nature Communications	123,958	12.124	0.722290
4	PROCEEDINGS OF THE NATIONAL ACADEMY OF SCIENCES OF THE UNITED STATES OF AMERICA	620,027	9.661	1.236860
5	National Science Review	512	8.843	0.002740
6	GigaScience	1,145	6.871	0.007590
7	Scientific Data	720	4.836	0.004690
8	Annals of the New York Academy of Sciences	44,545	4.706	0.039810
9	COMPLEXITY	1,429	4.621	0.002090
10	Scientific Reports	101,255	4.259	0.387610
11	Science Bulletin	1,087	4.000	0.003100
12	Journal of the Royal Society Interface	10,469	3.579	0.031990
13	Research Synthesis Methods	850	3.018	0.004300
14	PHILOSOPHICAL TRANSACTIONS OF THE ROYAL SOCIETY A-MATHEMATICAL PHYSICAL AND ENGINEERING SCIENCES	16,362	2.970	0.031980
15	PLoS One	508,248	2.806	1.924690
16	PROCEEDINGS OF THE JAPAN ACADEMY SERIES B-PHYSICAL AND BIOLOGICAL SCIENCES	1,162	2.324	0.002390
17	Royal Society Open Science	864	2.243	0.003380
18	SCIENCE AND ENGINEERING ETHICS	1,050	2.229	0.002780
19	NATURWISSENSCHAFTEN	6,601	2.221	0.004320
20	PeerJ	3,993	2.177	0.017790
21	PROCEEDINGS OF THE ROYAL SOCIETY A-MATHEMATICAL PHYSICAL AND ENGINEERING SCIENCES	16,771	2.146	0.016750
22	CHINESE SCIENCE BULLETIN	10,996	1.649	0.016680
23	Proceedings of the Romanian Academy Series A-Mathematics Physics Technical Sciences Information Science	334	1.623	0.000850
24	FRACTALS-COMPLEX GEOMETRY PATTERNS AND SCALING IN NATURE AND SOCIETY	887	1.540	0.000890

SCIENTIFIC REPORTS

Correction: Author Correction

OPEN

NMDA-receptor inhibition and oxidative stress during hippocampal maturation differentially alter parvalbumin expression and gamma-band activity

Received: 15 January 2018
Accepted: 11 June 2018
Published online: 22 June 2018

Luisa A. Hasam-Henderson[1], Grace C. Gotti[1], Michele Mishto[3,4], Constantin Klisch[1], Zoltan Gerevich[1], Jörg R. P. Geiger[1,2] & Richard Kovács[1]

Dysfunction of parvalbumin (PV)-expressing interneurons is thought to underlie the alterations of gamma-band oscillations observed in schizophrenia. Although the pathomechanisms of this disease remain unclear, oxidative stress induced by NMDA receptor (NMDAR) hypofunction and decreased glutathione (GSH) synthesizing capacity have been shown to lead to PV-loss and aberrant oscillatory activity. However, the individual contributions of NMDAR-inhibition and GSH-depletion to the developmental alterations observed in schizophrenia are largely unknown. We therefore investigated each condition in isolation using hippocampal slice cultures wherein interneuron maturation occurs entirely *in vitro*. Although both treatments caused oxidative stress, NMDAR-inhibition led to an immediate reduction in gamma oscillation frequency and a delayed loss of PV. In contrast, GSH-depletion immediately decreased PV expression and increased power, without affecting frequency. Hence, although disturbances of PV-expression and gamma oscillations coexist in schizophrenia, they can arise from separate pathological processes.

Schizophrenia is a common neurodevelopmental disorder affecting ~1% of the population with symptoms typically appearing in late adolescence and early adulthood[1]. Current pharmacotherapy non-selectively targets the dopamine receptor D2, primarily ameliorating the positive symptoms (delusions and hallucinations) while improvement of the negative and cognitive symptoms (affective flattening, social withdrawal, memory problems) remains a challenge[1,2]. Information processing and exchange within and between brain regions rely on the synchrony of neural activity, manifested as oscillations in the EEG. In schizophrenia, altered gamma-band activity (30–80 Hz) is indicative of network function disturbances and correlates with the severity of symptoms[3,4]. Parvalbumin positive (PV+) fast-spiking GABAergic interneurons mediate perisomatic inhibition and determine the timing of pyramidal cell firing[5], which is critical for synchronization of neuronal ensembles during certain forms of gamma activity[6–12]. Altered functional properties of these interneurons, as well as decreased expression of PV and the GABA synthesizing enzyme glutamic acid decarboxylase-67 (GAD67), have been described in individuals affected by schizophrenia and in animal models of the disease[13,14].

Although the etiology of these alterations is not fully understood, several lines of evidence suggest that NMDAR hypofunction during development might underlie the disturbances of network activity. Numerous genetic risk factors of schizophrenia are related to NMDAR signaling and it has been shown that early postnatal deletion of NMDAR not only disturbs cortical oscillations in the theta/gamma range but also decreases PV and

[1]Institut für Neurophysiologie, Charité – Universitätsmedizin Berlin, corporate member of Freie Universität Berlin, Humboldt-Universität zu Berlin, and Berlin Institute of Health, Berlin, Charité Platz 1, 10117, Berlin, Germany. [2]The NeuroCure Cluster of Excellence, Berlin, Germany. [3]Institut für Biochemie, Charité – Universitätsmedizin Berlin, corporate member of Freie Universität Berlin, Humboldt-Universität zu Berlin, and Berlin Institute of Health, Berlin, Charité Platz 1, 10117, Berlin, Germany. [4]Centre for Inflammation Biology and Cancer Immunology (CIBCI) & Peter Gorer Department of Immunobiology, King's College London, SE1 1UL, London, United Kingdom. Correspondence and requests for materials should be addressed to R.K. (email: richard.kovacs@charite.de)

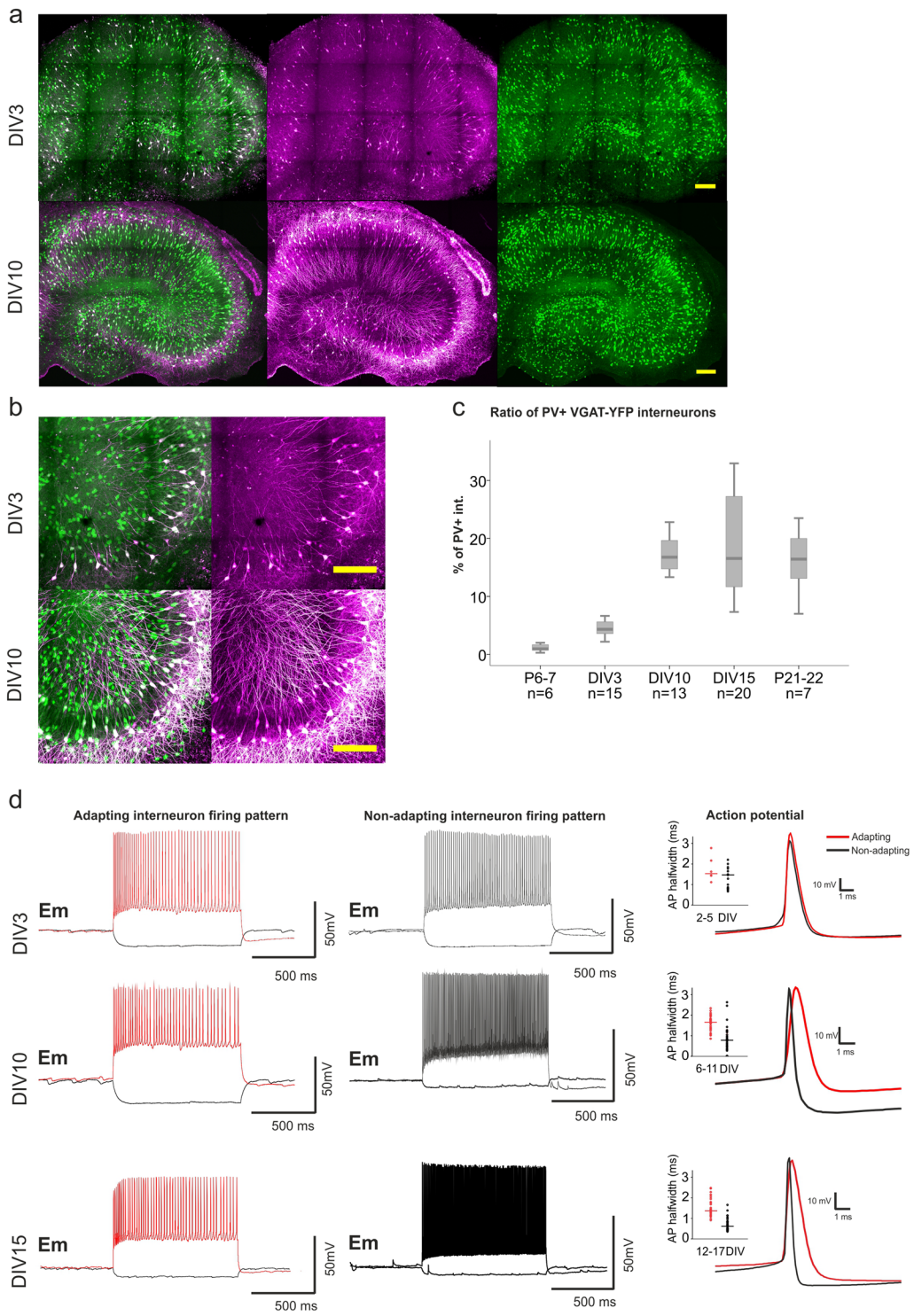

Figure 1. Changes in PV expression and electrophysiological properties of adapting and non-adapting interneurons during slice culture development. Slice cultures of VGAT-YFP rats were labelled for PV at different developmental time points. (**a**,**b**) Representative hippocampal images of DIV3 and DIV10 hippocampal slice cultures (**a**) and respective close ups to the CA3 region are shown (**b**). VGAT-YFP expressing interneurons are displayed in green and PV+ interneurons in magenta (scale bar 200 µm). (**c**) Boxplot depicting in percentage the ratio of YFP+/PV expressing interneurons after 3, 10 and 15 DIV (4.31, 16.76 and 16.54%), and in acute slices at postnatal day (P) 7 and 21–22 (corresponding to DIV15) (0.95 and 16.43%). For each *in vitro* developmental time point hippocampal slices were obtained from 5–6 rats, while for acute slices 3–4 animals were used. The ratio was calculated by counting the total hippocampal number of YFP+ interneurons and PV-labelled interneurons per slice in the 3D reconstruction. (**d**) Exemplary traces of firing patterns upon a 1 s long depolarization step of adapting (red) and non-adapting (black) interneurons are shown for slice cultures at DIV3, 10 and 15. Representative single action potentials of adapting and non-adapting interneurons taken

at different developmental stages (DIV2–5; 6–11, 12–17) (right), the excerpt shows the distribution of action potential width at half maximum of AP amplitude (half-width) for respective cell groups. Cells (164) were recorded from 70 slices obtained from 32 animals (for a detailed description of the *in vitro* maturation of electrophysiological properties see Supplementary Fig. 1).

GAD67 expression[15,16]. Previous studies have reported that perinatal NMDAR hypofunction alters interneuron development by eliciting oxidative stress[1]. A direct link between NMDAR hypofunction and oxidative stress was established in a model of acute psychosis induced by the NMDAR antagonist, ketamine, where the loss of the fast spiking phenotype and PV expression in interneurons was associated with the activation of the superoxide producing enzyme, NADPH-oxidase 2 (NOX2)[17]. In addition, the antioxidant N-acetyl-cysteine (Nac) was able to prevent the consequences of NMDAR hypofunction following ventral hippocampus lesion on PV interneuron activity and ameliorated behavioral deficits[18].

The contribution of oxidative stress to schizophrenia is further supported by the fact that decreased levels of the small molecular antioxidant glutathione (GSH) is a common finding in schizophrenia patients[13,19], whereas adjunctive treatment with the antioxidant GSH precursor (Nac) improves the negative symptoms[20]. Indeed, polymorphism analysis of the GSH-synthesizing enzyme, glutamate-cysteine ligase, revealed that certain alleles are associated with a higher risk of developing schizophrenia[21]. In animal models, mutations of the GSH-synthesizing enzyme are sufficient to decrease PV expression and change the GABAergic phenotype of interneurons, resulting in aberrant gamma oscillations as well as altered affective behaviour[22,23].

The positive correlation between synaptic NMDAR activation and GSH synthesis[24] intuitively links NMDAR hypofunction to decreased GSH levels[25]. Currently, it is still unclear whether the network and interneuron alterations in schizophrenia represent direct consequences of NMDAR hypofunction or if they are downstream from the NMDAR hypofunction-induced oxidative stress.

In this study, we test the hypothesis that NMDAR hypofunction and redox imbalance of the GSH system stereotypically alter the maturation of the neuronal network activity.

Since the alterations in PV+ interneuron properties that underlie the aberrant gamma band activity occur during early perinatal development, we used slice cultures where the maturation of interneurons takes place entirely *ex vivo*[26–29]. Cultures were obtained from transgenic Wistar rats expressing Venus-YFP on the vesicular γ-aminobutyric acid transporter (VGAT) promoter[30], thereby allowing the identification of changes in the interneuron population following either NMDAR-inhibition or GSH depletion. By assessing total tissue GSH and oxidized protein levels, as well as gamma oscillation properties and PV expression at different time points during development, we investigate whether NMDAR inhibition would induce oxidative stress and alter GSH levels and if the resulting changes in gamma oscillation and PV expression would be comparable to those elicited by direct inhibition of GSH synthesis.

Results

Characterization of the *ex vivo* maturation of the hippocampal network activity and PV+ interneurons. In order to investigate the effects of NMDAR inhibition and oxidative stress in isolation, we first characterized the *in vitro* maturation of interneurons and the neuronal network in hippocampal slice cultures.

To rule out that the culturing *per se* would alter PV expression in the hippocampus, first we characterized its expression pattern at three different time points i.e. days *in vitro* (DIV) 3 (n = 15), 10 (n = 13) and 15 (n = 20) and compared it to that of age matched acute slices (at P7 (n = 6) and P21–22 (n = 7)), which would represent the intact development of PV expression). Even though PV+ interneuron migration is complete by the time of slice preparation (P7), PV identification is limited as the protein is still barely expressed[31]. Using multiphoton microscopy and 3D reconstructions of the entire hippocampal slice culture, we quantified for each slice the total hippocampal number of YFP+ and PV-labelled interneurons and calculated the ratio of YPF+ interneurons expressing PV (presented in percentage). Indeed, we observed a time-dependent increase of PV labelling following explantation at P7 (DIV0), time point at which only 1% of the interneurons were PV+. By DIV3, 4% of the interneurons expressed PV, rising to 17% by DIV10 (Fig. 1a–c). This percentage remained stable at DIV15 (16.5%). These values were comparable to those observed in age-matched acute slices (16.4%) (P21–22 vs DIV15; $p = 0.699$; Fig. 1c), indicating that, despite the model-intrinsic slice thinning and broadening of the pyramidal cell layers during cultivation, PV expression continues to develop in slice cultures.

At the age of slice explantation, the electrophysiological properties of PV+ interneurons decisively differ from the adult characteristics, which in rodents reach complete maturity around postnatal day 25–28[4,32]. Since in our experimental setting the maturation process takes place under culture conditions, we first characterized the developmental changes in passive and active electrophysiological properties of VGAT-YFP-interneurons. Whole-cell patch clamp recordings were carried out at different time points ranging from DIV2 to 17. Interneurons recorded from the str. pyramidale - str. oriens border were divided into adapting and fast-spiking/non-adapting interneurons, based on their firing pattern (inter-event intervals between the first and last five action potentials (AP) in an AP train) (Fig. 1d). With increasing DIV, both interneuron groups showed a statistically significant ($p < 0.01$) negative correlation of membrane resistance (two-tailed Spearman correlations, ρ: −0.485 and ρ: −0.351) and a positive correlation of membrane capacitance (ρ: 0.368 and ρ: 0.306, for non-adapting and adapting, respectively) likely indicating neuronal growth/arborization in culture (Supplementary Ia and b). In adapting interneurons, AP-frequency and AP-half-width did not change significantly. By contrast, in non-adapting interneurons the maximum AP-frequency and AP-half-width showed a strong correlation with DIV, where the maximum frequency

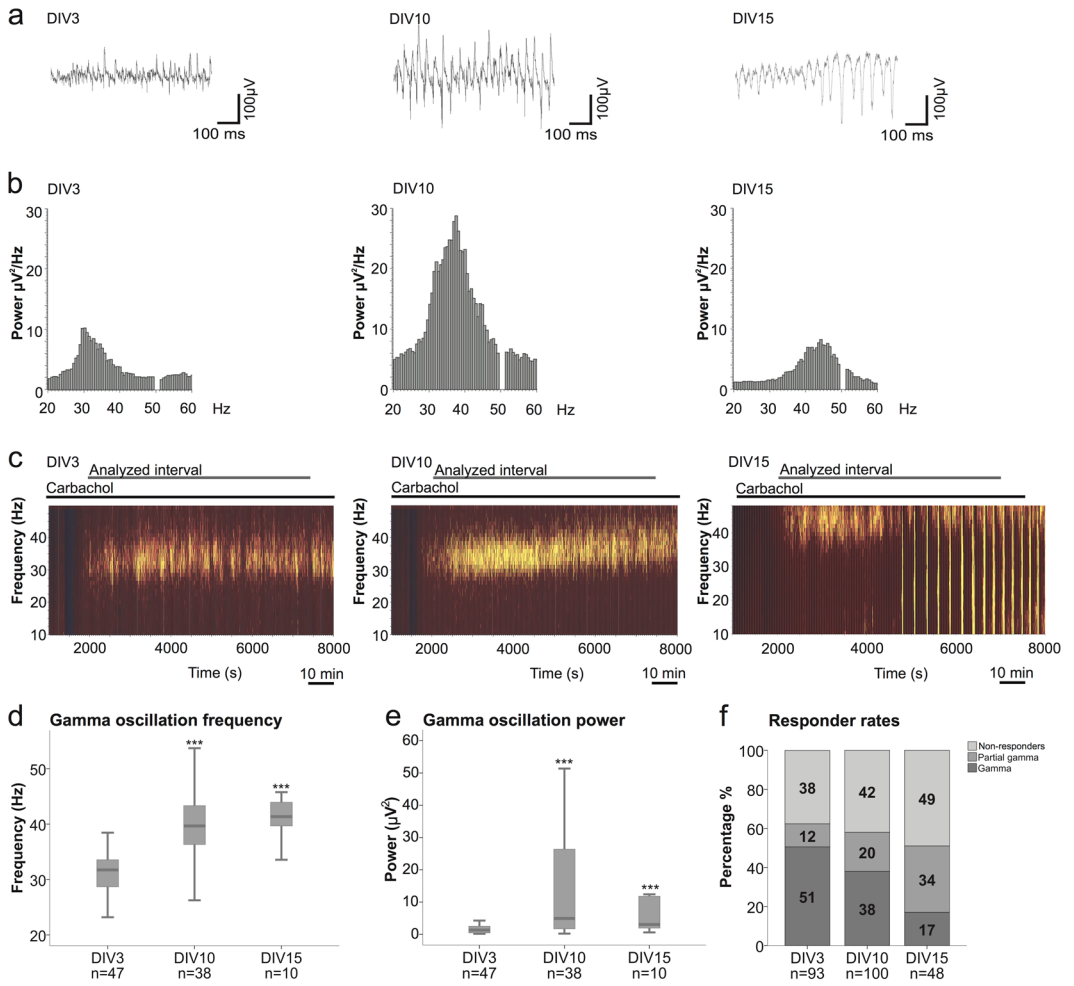

Figure 2. *In vitro* maturation of network activity. (**a**) Exemplary field potential traces of carbachol (Cch) induced gamma oscillations at DIV3 (left), DIV10 (middle) and DIV15 (right). In the DIV15 excerpt, the transition from gamma oscillations to epileptiform discharges are depicted. (**b**) Representative power spectra (window size: 120 s) of gamma oscillations at DIV3 (left), DIV10 (middle) and DIV15 (right). (**c**) Representative sonograms of local field potential recordings obtained from DIV3 (left), DIV10 (middle) and DIV15 (right) slices during gamma oscillations. An example of gamma oscillations intermingled with spontaneous discharges observed in DIV15 cultures is shown in the right sonogram. (**d**,**e**) Boxplots presenting the gamma oscillation median of peak frequency and power in a 90 min period (from 2000–7400 s recording interval) at DIV3, 10 and 15 (DIV3: 31.7 Hz, 1.3 μV^2, DIV10: 39.7 Hz, 4.9 μV^2, DIV15: 41.4 Hz, 3 μV^2). The number of slices (n) are indicated in the plots. The number of animals used are as follows: 30, 31 and 8 rats for DIV3, 10 and 15, respectively. Kruskal-Wallis test and post-hoc Mann-Whitney U test was used for the comparison between DIV3 and DIV10/15 (***$p < 0.001$). (**f**) Responder rates of Cch-induced gamma oscillations are described for the three developmental time points (DIV3, 10 and 15). The number of slices displaying continuous gamma oscillations (gamma), discontinuous gamma oscillations (partial gamma) and non-responder slices (non-responders) are presented in percentage. For statistical analysis the two-tailed Fisher's exact test was performed.

became higher (ρ: 0.657) and the APs narrower (ρ: −0.428), reaching a value of 152.5 ± 8 Hz and 0.7 ± 0.03 ms after 9 days in culture ($p < 0.01$). These parameters remained stable up to DIV15 (Supplementary Ic and d).

We assessed the development of the hippocampal network by performing local field potential recordings (CA3) of carbachol (Cch)-induced gamma oscillations at three developmental time points: DIV3, 10 and 15. The peak frequency and power of a recording interval of 90 minutes (from 2000–7400 s) were calculated for the slices displaying oscillatory activity. We observed an increase in both, peak frequency and power from DIV3 to DIV10, which remained stable by DIV15 (Fig. 2d and e). The peak frequency rose from a median of 32 Hz at DIV3 to 40 Hz at DIV10 ($p = 5.62^{-10}$, $n = 47$ and 38, Mann-Whitney U test) with no further changes by DIV15 (41 Hz, $n = 10$, $p = 0.4536$, Mann-Whitney U test). Similarly, the peak power increased significantly from DIV3 to DIV10 (Mdn 1.3 μV^2, 4.9 μV^2, $p = 1.5^{-5}$, $n = 47$ and 38, Mann-Whitney U test), while no significant increase was observed between DIV10 and 15 (Mdn 4.9 μV^2, 3.1 μV^2, $n = 38$ and 10, $p = 0.4022$, Mann-Whitney U test) (Fig. 2d and e) (Detailed statistical analysis is shown in supplementary material). Interestingly, the ability of the cultures to sustain continuous gamma oscillations throughout the 90 min period declined gradually with time in culture. At DIV3, 51% of the slices showed persistent oscillations dropping to only 17% at DIV15 (Fig. 2f). Longer time in

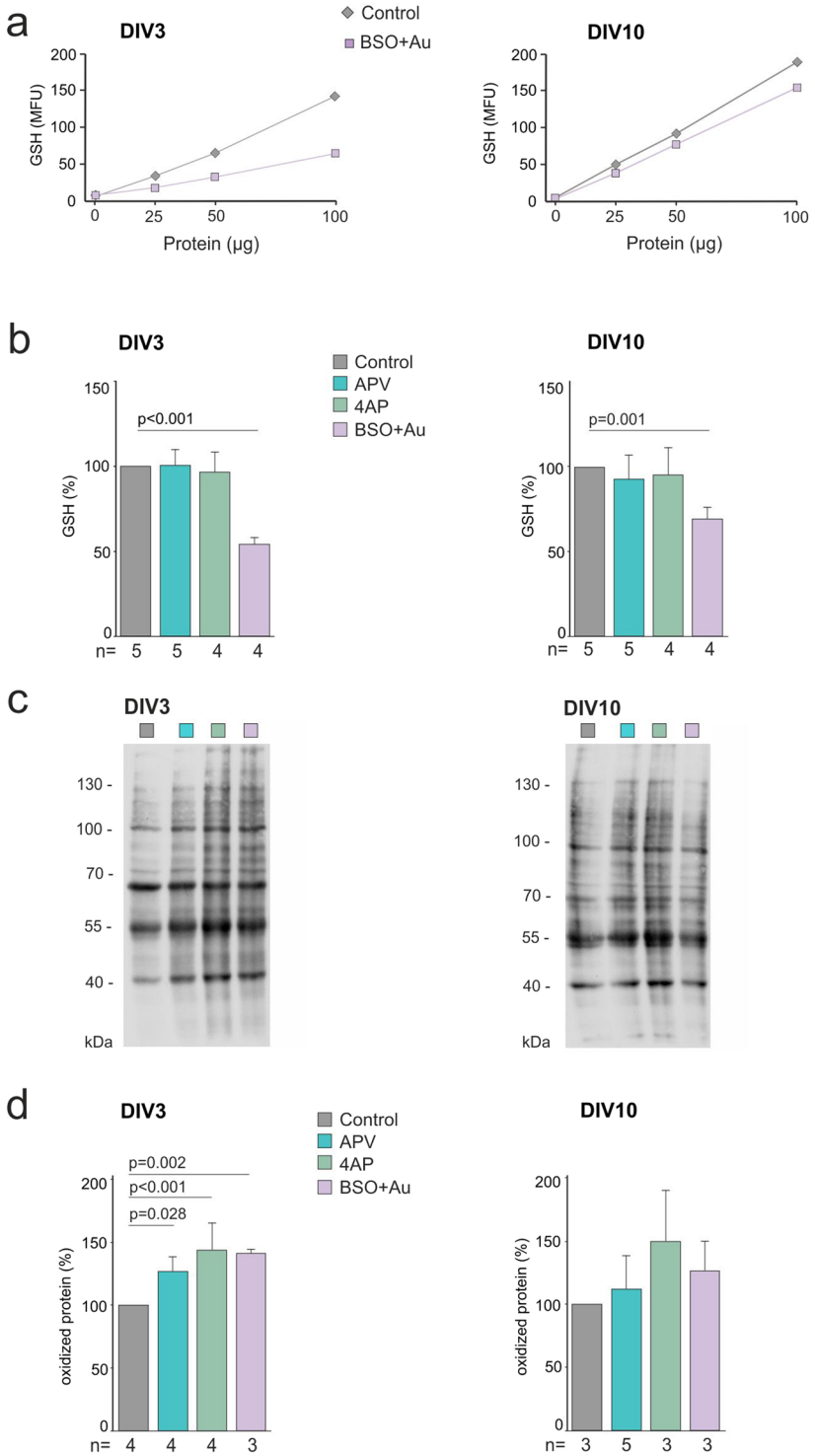

Figure 3. Effects of NMDAR inhibition, oxidative stress and increased synaptic activity on total GSH content and on protein oxidation levels. (**a**) Representative examples of the linear correlation between the GSH levels (measured as mBCI fluorescence) and the protein concentration in the cell lysate of DIV3 (left) and 10 (right) in control and BSO/Au treated (oxidative stress) slice cultures. (**b**) Quantification of the relative GSH content after APV, 4AP and BSO/Au treatments at DIV3 (left) (Control 100; APV 102.8 ± 8.7; 4AP 96.5 ± 12; BSO/Au 55.3 ± 4.3, $p = 8.12^{-8}$, mean ± SD, ANOVA, post-hoc Bonferroni) and DIV10 (right) (Control 100; APV 93 ± 14.4; 4AP 95.4 ± 16.2; BSO/Au 72.3 ± 8.9, p = 0.001, mean ± SD, ANOVA, post-hoc Bonferroni). All treatments started at DIV1 and the drugs were present throughout the development. The number of independent experiments (n) are shown in the figures, for each experiment (4 or 5) 9–18 slice cultures from 3–4 rats were used. (**c**) Representative oxyblot (of 3–4 independent experiments) presenting oxidized protein level in cell lysates at DIV3 (left) and 10 (right) in control and treated slice cultures. Full-length gels are included in the supplementary material. (**d**) Relative oxidized protein levels in control and treated slice cultures at DIV3

(left) (Control 100; APV 126.8 ± 11.5, p = 0.028; 4AP 144.1 ± 19.1, p = 3.5^{-5}; BSO/Au 141.2 ± 4, p = 0.002; mean ± SD, ANOVA, post-hoc Bonferroni) or DIV10 (right) (Control 100; APV 112.1 ± 26.3; 4AP 149.7 ± 40.2; BSO/Au 126.6 ± 23.2, ANOVA, post-hoc Bonferroni). For each experiment (n) 9–18 slice cultures from 3–4 rats were used. Significant differences between groups are marked with the respective p values (Anova test with Bonferroni correction for multiple comparisons).

culture induced a shift to shorter periods of gamma oscillations (partial gammas), which were often followed by a switch into recurrent discharges, resembling epileptiform activity (Fig. 2a right and c right). Only slices with continuous gamma oscillations for the given 90 min interval were included in the analysis. Thus, extending the study until DIV15 did not provide additional information, due to increasing propensity to epileptiform discharges.

Fast-spiking PV+ interneurons are indispensable for maintaining synchronicity during Cch-induced gamma oscillations in the CA3 region[6–9]. Therefore, the gradual increase in frequency between DIV3 and DIV10 might correlate with the observed changes in the electrophysiological properties of non-adapting interneurons. Together, these results suggested that interneuron and network maturation reaches a plateau by DIV10, suggesting an experimental window for treatment prior to this time point.

Drug application for NMDAR inhibition and induction of oxidative stress. Following the characterization of the maturation of hippocampal slice cultures, we proceeded to simulate NMDAR hypofunction or GSH-depletion in a developmental window from DIV1-10. Slice cultures were exposed either to the selective NMDAR antagonist DL-2-Amino-5-phosphonopentanoic acid (APV, 50 µM), or to a combined application of buthionine sulfoximine (BSO), an inhibitor of γ-glutamylcysteine synthetase (γ-GCS), the rate-limiting enzyme of GSH synthesis, and Auranofin (Au), a thioredoxin reductase inhibitor[33]. We have chosen to block the Peroxiredoxin/Thioredoxin/Thioredoxin-reductase antioxidant system (TRX) in parallel to γ-GCS, as it was shown to contribute to the peroxide detoxification[33], and to compensate for the effect of GSH deprivation[34,35]. The short and long term effects of each treatment on total tissue GSH content, oxidized protein levels, gamma oscillations and PV expression were assessed at an early (DIV3) and a late (DIV10) developmental stage. For all cases, slices were exposed to the inhibitors during the entire culture period starting from DIV1 but they were withdrawn during the induction and recording of gamma oscillations.

NMDAR inhibition increases protein oxidation without affecting GSH levels. In the first set of experiments, we investigated whether NMDAR inhibition would induce oxidative stress and reduce the total tissue GSH content, comparable to the partial blockade of the GSH synthesis by BSO. In order to determine a tolerable level of GSH-depletion that would not interfere with slice viability, four different BSO concentrations (0.5, 1, 5, 10 µM) were tested. While BSO was lethal at concentrations above 5 µM, inducing swelling and cell loss after overnight exposure, slices treated with BSO/Au (1 µM–1 µM) remained viable for as long as DIV15. GSH levels were determined spectrophotometrically from slice lysates by measuring the fluorescent adduct of monochlorobimane (mBCI) following the reaction with glutathione-S-transferase[24]. BSO/Au exposure resulted in a ~45% reduction of GSH levels at DIV3 (GSH level was 55.3 ± 4.3% of the control, n = 5, 4 independent experiments for control and BSO/Au, respectively, p < 0.001, mean ± SD, ANOVA, Bonferroni post-hoc) and 31% at DIV10 (GSH level was 72,3 ± 8.9% of the control, n = 5, 4, independent experiments for control and BSO/Au, p = 0.001, ANOVA, Bonferroni post-hoc) (Fig. 3b). In contrast, NMDAR inhibition by APV did not change the total tissue GSH levels, neither at DIV3 (n = 5) nor at DIV10 (n = 5), suggesting that NMDAR activity is not indispensable for the maintenance of basal GSH synthesis (Fig. 3b). Subsequent confocal imaging of the fluorescent mBCI-GSH adduct in intact slice cultures confirmed previous studies reporting higher cytosolic GSH concentrations in putative glial cells than in neurons[36] (Supplementary Fig. 2a). Thus, the inability of APV to change GSH levels indicates that total tissue GSH is largely determined by the glial compartment and independent of NMDAR activity.

Despite the unchanged GSH levels, NMDAR inhibition might still induce oxidative stress in neurons, which might have remained undetected in the previous experimental setting. We therefore proceeded to assess protein oxidation in slice cultures via oxyblot assay, which labels the carbonyl groups introduced into proteins by oxidative reactions. We observed an increase in protein oxidation at DIV3 in both the APV and BSO/Au treated groups (APV: 126.8 ± 11.5%, p = 0.028; BSO/Au, 141.2 ± 4%, p = 0.002, mean ± SD, oxidized proteins in percentage of the control, n = 4, 4, 3 independent experiments, ANOVA, Bonferroni post-hoc), as compared to age-matched control slice cultures (Fig. 3d). However, despite the continuous exposure to the inhibitors, the effects were not maintained and no significant increase in oxidized proteins was observed at DIV10 (APV: 112.1 ± 26.3%, p = 1; BSO/Au: 126.6 ± 23.2%, mean ± SD, p = 1, n = 3, 5, 3 independent experiments, ANOVA, Bonferroni post-hoc) (Fig. 3d). To investigate whether the initial increase might be intrinsic to the slice model and the culturing conditions, we analyzed the time course of protein oxidation (DIV0 4, 7, 10) in untreated cultures. The amount of oxidized proteins gradually increased following explantation (P7-DIV0), peaking at DIV7 and recovering to a less oxidized state at DIV10 (Supplementary Fig. 2b). These results point to the presence of an intrinsic adaptive antioxidant response and enhanced removal of oxidized proteins after DIV7, probably also boosting the recovery from the oxidative stress induced by BSO/Au or APV.

NMDAR antagonism decreases the frequency of gamma oscillations before reducing PV expression. Previous studies have reported a decrease in PV expression after acute and chronic NMDAR hypoactivity *in vivo* in different brain regions[15,37]. Therefore, we investigated whether the same trend could be observed in our model. Exposing slices to APV gradually decreased PV expression reaching statistical significance by DIV10 (Control Mdn 16.8, n = 13; APV Mdn 13.1, n = 10, p = 0.0256, Mann-Whitney U test) (Fig. 4a and b right). At

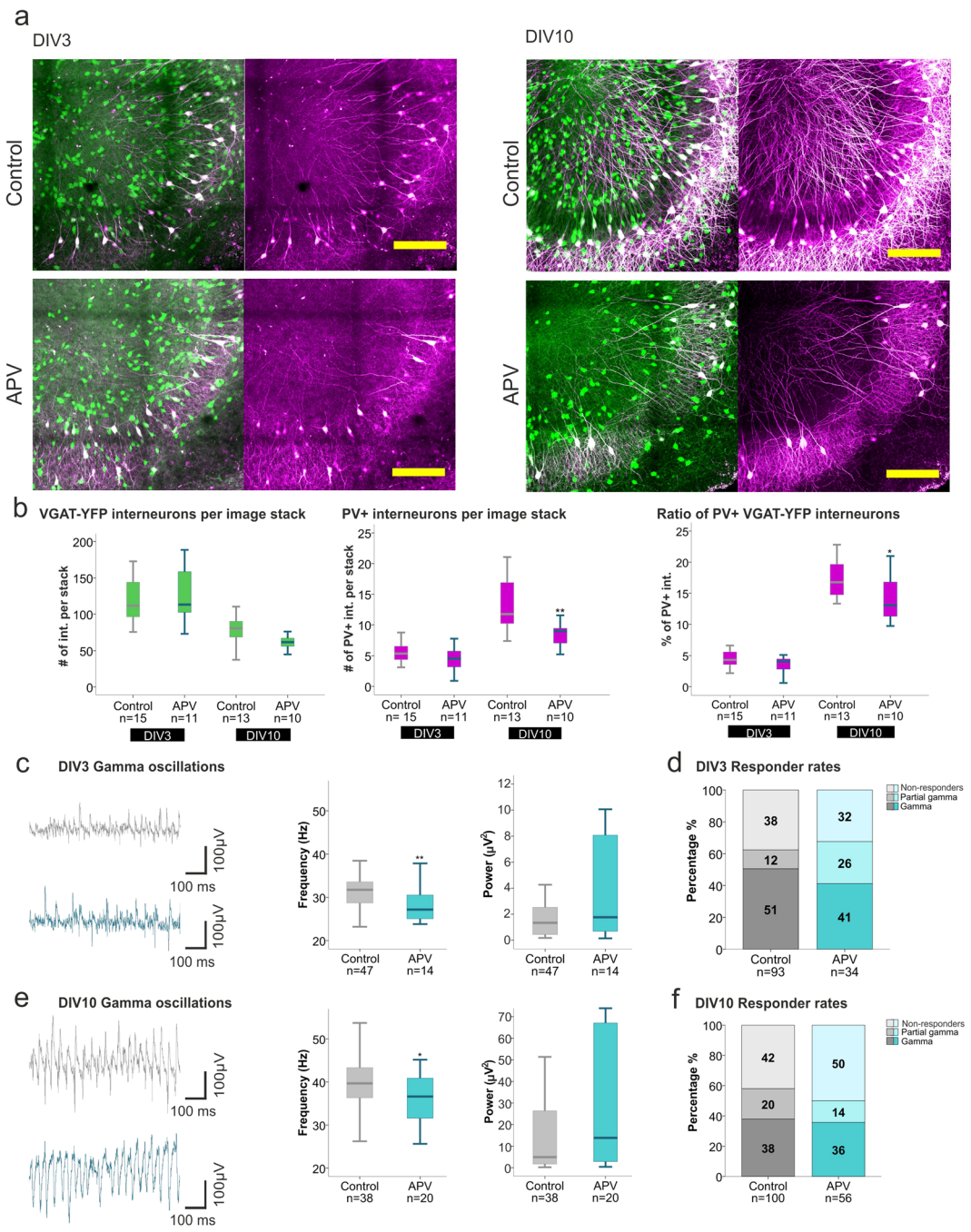

Figure 4. Effects of NMDAR inhibition on PV expression and gamma oscillations. (**a**) Representative images of the hippocampal CA3 region of control and APV treated slices at DIV3 (left) and 10 (right), depicting VGAT-YFP interneurons (green) and PV labelled interneurons (magenta) (scale bar 200 µm). (**b**) Boxplots presenting the median of the number of VGAT-YFP interneurons (left) (DIV3 control 111.8, APV 113.2, DIV10 control 80.5, APV 61.8) and PV+ interneurons (middle) (DIV3 control 5.3, APV 4.5, DIV10 control 11.8, APV 8.9) per focal plane as well as the ratio of PV+/YFP+ interneurons in the 3D hippocampal slice (right) (DIV3 control 4.3%, APV 4.1%, DIV10 control 16.8%, APV 13.1%) for control and APV treated slices, at DIV3 and 10. Hippocampal slices were prepared from 5–6 rats per group. The Mann-Whitney U test was used for statistical analysis (*$p < 0.05$, **$p < 0.01$). (**c**,**e**) Boxplots presenting the gamma oscillation peak frequency and power of control and APV treated slices at DIV3 (**c**) (control 31.7 Hz, 1.3 μV^2, APV 27.2 Hz, 1.8 μV^2) and DIV10 (**e**) (control: 39.7 Hz, 4.9 μV^2; APV: 36.6 Hz, 13.8 μV^2). The number of animals used for the control and APV-treated slice preparation are as follows: DIV3; 30 and 10 rats, DIV10; 31 and 13 rats. Statistical analysis was performed using the Mann-Whitney U test on the respective median values (calculated from the 2000–7400 s interval) (*$p < 0.05$, **$p < 0.01$). (**d**,**f**) Responder rates to Cch of control and APV treated slice cultures at DIV3 (**d**) and 10 (**f**). Statistical analysis was performed using the two-tailed Fisher's exact test including the three categories of activity (gamma, partial gamma and non-responders).

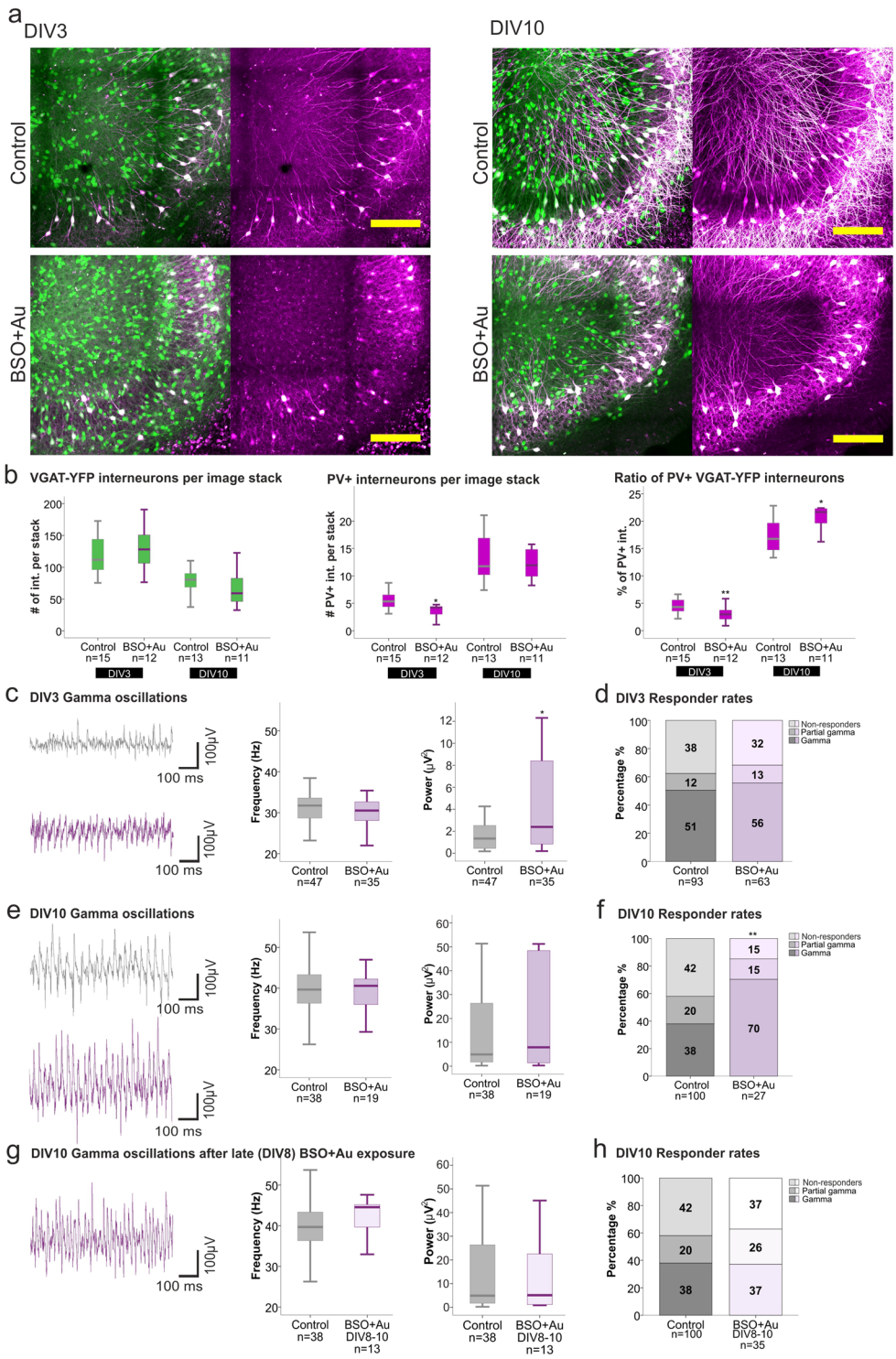

Figure 5. Effects of oxidative stress on PV expression and gamma oscillations. (**a**) Representative images of the hippocampal CA3 region of control and BSO/Au treated slices at DIV3 (left) and 10 (right), depicting VGAT-YFP interneurons (green) and PV+ interneurons (magenta) (scale bar 200 μm). (**b**) Boxplots presenting the median of the number of VGAT-YFP interneurons (left) (DIV3 control 111.8, BSO/Au 128.1, DIV10 control 80.5, BSO/Au 59.1) and PV+ interneurons (middle) (DIV10 control 5.3, BSO/Au 4.2, DIV10 control 11.8, BSO/Au 11.9) per focal plane as well as the ratio of PV+/YFP+ interneurons in the 3D hippocampal slice (right) (DIV3 control 4.3%, BSO/Au 3%, DIV10 control 16.8%, BSO/Au 21.7%) for control and BSO/Au treated slices, at DIV3 and 10. Hippocampal slices were prepared from 5–6 rats per group. The Mann-Whitney U test was used for statistical analysis (*$p < 0.05$, **$p < 0.01$). (**c**,**e**,**g**) Boxplots present the median of the gamma oscillation peak frequency and power of control and BSO/Au treated slices at DIV3 (**c**) (control: 31.7 Hz, 1.3 μV^2, BSO/Au: 30.5 Hz, 2.3 μV^2) and DIV10 (**e**) (control: 39.7 Hz, 4.9 μV^2; BSO/Au: 40.6 Hz, 7.9 μV^2). The peak frequency and power of gamma oscillations in slices exposed to BSO/Au in later stages of development (from DIV8-10)

are also displayed (control: 39.7 Hz, 4.9 μV^2; BSO/Au 44.6 Hz, 5.1 μV^2) (**g**). The number of animals used for the control, early exposure BSO/Au treatment and late exposure BSO/Au treatment are as follow: DIV3; 30 and 9 rats, DIV10; 31, 15 and 6 rats. Statistical analysis was performed using the Mann-Whitney U test on the medians (calculated from the 2000–7400 s recording interval) of responding slices (*$p < 0.05$). (**d**,**f**,**h**) Responder rates to Cch of control and BSO/Au treated slices recorded at DIV3 (**d**) and 10 (**f**), as well as for late BSO/Au treatment (DIV8-10) (**h**) are given as percentage of all slices investigated. Statistical analysis was performed using the two tailed Fisher's exact test including the three categories of activity (gamma, partial gamma and non-responders).

this developmental time point a tendency to a decrease in the absolute number of interneurons was detectable when compared to controls (Control Mdn 80.5; APV Mdn 61.8, $p = 0.0628$, Mann-Whitney U test), indicating a long-term negative effect of NMDAR inhibition on the interneuron survival (Fig. 4b left).

Previous evidence suggests that the loss of PV goes along with alterations in the electrophysiological properties of interneurons[15,17]. In the next set of experiments, we investigated whether the decreased PV expression induced by APV would also reflect on the hippocampal network activity. Already by DIV3, we observed a marked decrease in the peak frequency of the Cch-induced gamma oscillations (Control Mdn 31.7 Hz, $n = 47$; APV Mdn 27.2 Hz, $n = 14$, $p = 0.0031$, Mann-Whitney U test), despite the absence of a significant change in PV expression or absolute numbers of interneurons. This decrease in frequency was maintained up to DIV10 (Control Mdn 39.7 Hz, $n = 38$; APV Mdn 36.6 Hz, $n = 14$, $p = 0.0254$, Mann-Whitney U test). No overt changes in the power of gamma oscillations were detected at any assessed time point (Fig. 4c and e). Detailed statistics are included in supplementary material. Furthermore, NMDAR inhibition did not alter the propensity of the slices to develop gamma oscillations, which was comparable to that of the control groups (DIV3 $p = 0.1543$, $n = 93$ and 34; DIV10 $p = 0.5733$, $n = 100$ and 56, Fisher's exact test two-tailed) (Fig. 4d and f).

Thus, NMDAR inhibition in slice cultures emulates the reduced PV expression and altered gamma oscillation frequency observed *in vivo* after perinatal exposure to NMDAR antagonists[38]. However, in our setting, the alterations in the gamma-band activity precede the loss of PV expression in interneurons.

Oxidative stress disturbs PV expression while transiently increasing gamma oscillation power. In the following set of experiments we investigated whether oxidative stress alone would mimic the alterations observed following NMDAR inhibition. Partial inhibition of the GSH synthesis and Trx-reductase activity reduced the number of PV+ interneurons at DIV3 (Control Mdn 5.3, $n = 15$; BSO/Au Mdn 4.2, $n = 12$, $p = 0.0112$, Mann-Whitney U test) without affecting the overall number of interneurons (Fig. 5a and b left and middle). The remaining PV+ interneurons presented truncated dendrites. However, at DIV10 the PV expression was increased again and the PV+/YFP ratio was restored to control levels. While at this time point the number of PV+ interneurons per focal plane in treated slices was similar to that observed in controls (Control Mdn 11.8, $n = 13$; BSO/Au Mdn11.9, $n = 11$, $p = 0.7856$, Mann-Whitney U test), the rise in the ratio hints to a moderate interneuron loss still not reaching significance (Control Mdn 80.5, $n = 13$; BSO/Au Mdn 59.1, $n = 11$, $p = 0.2767$) (Fig. 5a and b left and middle). This lower interneuron count together with the unchanged number of PV+ interneuron explains the significant increase in the PV+/YFP+ interneurons ratio (Control Mdn 16.8, $n = 13$; BSO/Au 21.7, $n = 11$, $p = 0.0190$, Mann-Whitney U test) (Fig. 5b right). In fact, we observed an apparent thinning of slice cultures after long exposure to oxidative stress, suggesting general cell loss. Despite the marked reduction of PV expression after initial BSO/Au exposure (DIV3), the frequency of gamma oscillations remained unchanged while the power significantly increased (Control Mdn 1.3 μV^2, $n = 47$; BSO/Au Mdn 2.39 μV^2, $n = 35$, $p = 0.0273$, Mann-Whitney U test) (Fig. 5c and d), as opposed to the observations in cultures following NMDAR inhibition. Although at DIV10 the peak frequency and power remained similar to control levels, the prolonged oxidative stress almost doubled the responder rates, suggesting a higher ability to maintain continuous gamma band activity for periods longer than 90 min (Control 38%, $n = 100$ vs BSO/Au 70%, $n = 56$, $p = 0.0094$, two-tailed Fisher's exact test) (Fig. 5f).

As the disturbance in PV expression and the increased gamma power were only present following two-day exposure to BSO/Au, we proceeded to investigate whether these alterations were dependent on the developmental stage of the cultures or if they solely represented a stereotypic acute response to oxidative stress. To this end, we administered BSO/Au to DIV8 slices and assessed alterations of gamma oscillations at DIV10. In these slices the gamma frequency and power did not differ from those observed in the control group (Fig. 5g and h), indicating that the electrophysiological effects of the inhibition of GSH/Trx systems strongly depends on the developmental state of the neuronal network.

Based on these findings, we concluded that NMDAR inhibition and oxidative stress differentially alter network development with respect to the time course of PV reduction and the frequency of the gamma-band oscillatory activity

Increasing synaptic transmission improved interneuron survival despite enhanced protein oxidation. Activation of synaptic NMDAR is suggested to increase the capability of neurons to synthesize GSH and to cope with oxidative stress[24,39]. In the last set of experiments, we sought to determine if a general increase in neuronal activity would affect tissue GSH levels and reverse the effects of oxidative stress on the network maturation. To this end, we applied 4AP, a broad-spectrum inhibitor of voltage-gated potassium channels. Despite the enhanced network activity, GSH levels remained unchanged at both DIV3 ($p = 0.620$) and DIV10 ($p = 0.339$) (Fig. 3b and c). Remarkably, 4AP induced a significant increase in oxidized protein levels at DIV3 ($p = 0.019$). Nevertheless, at DIV10, the statistical significance was lost (Fig. 3c and d), which can be explained by the model-inherent decline of protein oxidation after the first week in culture (Supplementary Fig. 2). Thus,

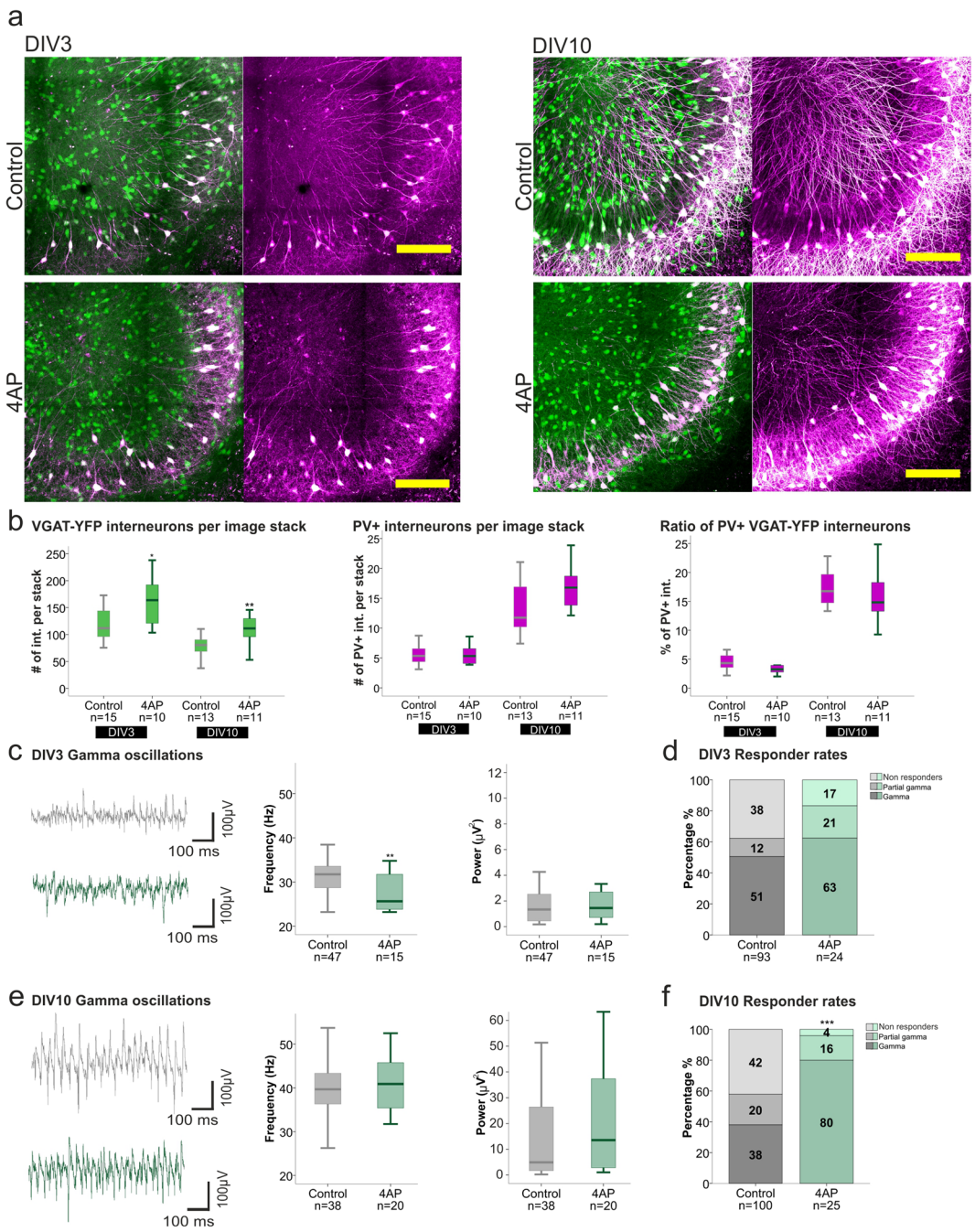

Figure 6. Effects of increased network activity on PV expression and gamma oscillations. (**a**) Representative images of the hippocampal CA3 region of control and 4AP treated slices at DIV3 (left) and 10 (right), depicting VGAT-YFP interneurons (green) and PV+ interneurons (magenta) (scale bar 200 µm). (**b**) Boxplots presenting the median of the number of VGAT-YFP interneurons (left) (DIV3 control 111.8, 4AP 163.8, DIV10 control 80.5, 4AP 111.4) and PV+ interneurons (middle) (DIV3 control 5.4, 4AP 5.3, DIV10 control 11.8, 4AP 16.8) per focal plane as well as the ratio of PV+/YFP+ interneurons in the 3D hippocampal slice (right) (DIV3 control 4.3%, 4AP 3.2%, DIV10 control 16.8%, 4AP 14.8%) for control and 4AP treated slices, at DIV3 and 10. Hippocampal slices were prepared from 5–6 rats per group. The Mann-Whitney U test was used for statistical analysis (*$p < 0.05$, **$p < 0.01$). (**c**,**e**) Boxplots present the median of the gamma oscillation peak frequency and power of control and 4AP treated slices at DIV3 (**c**) (control: 31.7 Hz, 1.3 μV^2, 4AP: 25.6 Hz, 1.5 μV^2) and DIV10 (**d**) (control: 39.7 Hz, 4.9 μV^2; 4AP: 40.9 Hz, 13.5 μV^2). The number of animals used for control and 4AP treated slices are as follow: DIV3; 30 and 10 rats, DIV10; 31 and 10 rats. Statistical analysis was performed using the Mann-Whitney U test on the medians of responding slices (**$p < 0.01$). (**d**,**f**) Responder rates to Cch of control and 4AP treated slices recorded at DIV3 (**d**) and 10 (**f**) are presented in percentage. Statistical analysis was performed using the two-tailed Fisher's exact test including the three categories of activity (gamma, partial gamma and non-responders).

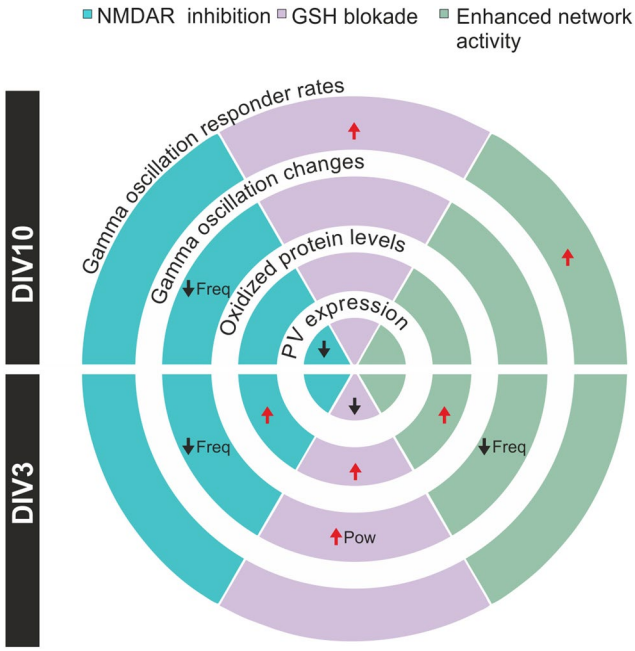

Figure 7. Summary of the changes in PV expression, protein oxidation, gamma oscillation properties and responder rates in the different treatment groups. Black arrows depict a significant decrease while red arrows indicate a significant increase. The segments without arrows were not statistically different from the control groups. The different treatments are depicted as follow: NMDAR-inhibition (APV exposure) in blue, oxidative stress (BSO/Au exposure) in purple and enhanced network activity (4AP exposure) in green.

enhancing network activity with 4AP did not alter the GSH synthesis but rather increased oxidative stress in our paradigm[40–42].

As PV expression and the fast-spiking phenotype of PV+ interneurons develop in an activity-dependent manner[28,43,44], we tested how the increased neuronal activity influenced these parameters in our model. Exposure to 4AP increased the number of interneurons throughout the culturing period (DIV3 control Mdn 111.8, n = 15; 4AP Mdn 163.8, n = 10, p = 0.0229; DIV10 control Mdn 80.5, n = 13; 4AP Mdn 111.4, n = 11, p = 0.0050, Mann-Whitney U test) (Fig. 6a and b), whereas the ratio of PV+/YFP+ interneurons did not change. As with NMDAR inhibition, 4AP also reduced the peak frequency of the gamma oscillations at DIV3 (Control Mdn 31.7 Hz, n = 47; 4AP Mdn 25.6 Hz, n = 15, p = 0.0054, Mann-Whitney U test). However, this drop in frequency was not accompanied by loss of PV phenotype, further substantiating that altered gamma oscillations and PV reduction are independent processes.

In contrast to the sustained effect of NMDAR inhibition on the frequency, in 4AP-exposed slices the gamma frequency recovered to control levels by DIV10 (Control Mdn 39.7 Hz, n = 38; 4AP Mdn 40.9 Hz, n = 20, p = 0.5392, Mann-Whitney U test) (Fig. 6c and e), along with an increase in the propensity to develop and maintain gamma oscillations. Responder rates doubled those observed in the control and APV treated groups (80%, 38% and 36% respectively). Interestingly, the increase in responder rates was similar to that displayed after prolonged oxidative stress due to BSO/Au exposure (DIV10) (70%, Fig. 6f). Thus, we propose that enhanced basal activity not only promoted interneuron survival, but in the long run also facilitated the induction of gamma oscillations.

Discussion

Early life NMDAR hypofunction induces oxidative stress in interneurons, leading to decreased PV and GAD67 expression as well as disturbances in the fast spiking phenotype[1,25,45,46]. These changes are thought to underlie the aberrant gamma oscillations and the cognitive/behavioral symptoms associated with schizophrenia[13,14]. Although NMDAR hypofunction and thiol redox imbalance are common findings in this pathology, their individual effects on developing neural circuitries had not yet been examined.

Here we report that NMDAR inhibition and GSH-depletion during early postnatal development distinctively alter gamma oscillations. While both treatments resulted in oxidative stress and decreased PV expression, this could either coincide or follow the changes in the network activity. Pharmacologically enhanced network activity led to altered gamma oscillations and increased protein oxidation, yet PV expression remained unchanged. Together these findings indicate that PV expression and alterations of gamma-band activity are not mutually interdependent, and general oxidative stress cannot be the common denominator of this pathology (Fig. 7).

The use of hippocampal slice cultures in this study allowed for individual and graded manipulation of NMDAR activity or GSH levels during maturation of the interneurons, which takes place following the time point (P7) for explantation[28,32,47]. Indeed, the electrophysiological properties (AP duration, maximum frequency) of non-adapting interneurons and the gamma oscillation frequency and power stabilized after the first week *in vitro*.

Moreover, the ratio of PV+ interneurons (Fig. 1c) as well as the properties of gamma band oscillatory activity corresponded those observed in age-matched acute slices, indicative of *ex vivo* interneuron and network maturation. Along with the progressive increase in power and frequency, the ability of slice cultures to maintain continuous gamma oscillations over 90 min declined with time *in vitro*. By DIV15, cultures displayed a higher propensity to shorter periods of oscillation intermingled with burst discharges. These changes could be due to the progressive neuron loss and increased axonal sprouting reported for aged slice cultures, which have been shown to facilitate the occurrence of epileptiform events[42,47,48]. Even though gamma oscillations are inducible in slice cultures up to DIV28[49] we curtailed the study at DIV10 before this deviation from the acute slice preparation would appear. Bearing in mind the differences due to the cultivation, slice cultures still represent a useful tool to study network development under different stressors.

The tripartite combination of NMDAR hypofunction, decreased PV+ expression and altered gamma oscillations has been associated to schizophrenia pathology[1,25,45,46]. While the cell type unspecific NMDAR inhibition by ketamine or phencyclidine decreases PV and GAD67 expression[15,17,38], selective genetic ablation of NMDAR on PV+ interneurons is sufficient to increase the power of gamma oscillations[16] and to trigger schizophrenia-like behavior[50,51].

Here we show that during early neuronal *in vitro* development, the exposure to a selective NMDAR inhibitior leads to an immediate and sustained decrease of the peak frequency of gamma oscillations, while reduction in PV expression occurs only after several days of treatment. This suggests that functional alterations in network activity might precede the downregulation of PV expression. The exact mechanisms by which NMDAR hypofunction disturb PV expression are not yet understood, however, oxidative stress has been suggested to contribute to PV loss[52] either via the activation of NOX[13,53–55] or by downregulating intrinsic antioxidant systems[51]. In our experimental setting, augmented levels of oxidized protein residues were observed following initial exposure to the NMDAR inhibitor, which, however, did not alter the PV expression. The loss in PV only became significant once the amount of oxidized protein had already recovered to control levels. This mismatch hints that general oxidative stress cannot be the main mechanism underlying the loss of PV phenotype.

GSH deficiency has frequently been reported in schizophrenia[1,19,21,22,53,56,57] and might contribute to the altered network activity by redox modification of the NR1 and NR2A subunits leading to impaired NMDAR function[25,58–60]. However, in our model a partial (~45%) depletion of the GSH pool (in the presence of Trx inhibition) did not mimic the effect of NMDAR inhibition on the network activity, despite the immediate suppression of PV expression. In contrast to NMDAR inhibition, GSH depletion induced a temporary increase in power, while the frequency remained unchanged. In the long run (at DIV10), gamma oscillation power and frequency returned to the control values but the responder rate was significantly higher. This is in line with the observation that a similar (~30–40%) decrease of the brain GSH content following *in vivo* blockade of GSH synthesis results in impaired synaptic signaling and plasticity[60] without having overt behavioral effects[61,62]. Thus decreased GSH content cannot account for the altered network activity observed in perinatal NMDAR hypofunction based models of schizophrenia. Remarkably, the increase in gamma power was only evident if GSH-depletion was applied during initial development of the cultures, whereas exposure to BSO after the first week *in vitro* (from DIV8 to 10) did not change gamma oscillation properties. The partial recovery of GSH levels from an initial ~45% reduction to a later ~30% in our model might come about from the upregulation of the antioxidant response element (ARE) genes inducing a compensatory GSH rise[63]. Another explanation might lay in the decrease of neuron/glia ratio (due to neuronal loss) increasing GSH availability as glial cells contain substantially more GSH than neurons[36].

The conclusion that general oxidative stress cannot mechanistically explain the effects of NMDAR hypofunction is further supported by the fact that enhanced network activity via 4AP augmented oxidized protein levels and decreased the frequency, without altering PV expression. Interestingly, oxidative stress induced by GSH depletion or by 4AP was associated with an increased propensity to express stable gamma oscillations indicating alterations of the interneuron population. While NMDAR inhibition and GSH depletion, if anything, reduced the total number of interneurons, network activity enhancement with 4AP promoted their survival. Although, the ratio of PV+/YFP interneurons in long-term GSH depleted cultures recovered and even surpassed the control values, this rise was due to a decrease in the absolute numbers of interneurons rather than a genuine increase in the number of PV+ interneurons. The better survival rate of PV+ interneurons in face of GSH-depletion suggests that these cells are more resistant to oxidative stress, which might be ascribed to the protective effects of the particularly dense perineuronal nets (PNN) surrounding PV+ interneurons[64]. Despite the continuous presence of BSO, the truncated dendrites of PV+ cells observed at DIV3 recovered by DIV10 (Fig. 4a,b), accompanied by an increase in the gamma oscillation responder rates. While fully developed PNN are known to limit new synapse formation and reorganization, PNN ablation reinstates developmental plasticity[65,66]. Thus, PNN disintegration resulting from increased oxidative stress might explain the observed recovery of dendritic/axonal arborization and probably the enhanced propensity to gamma oscillations.

In case of enhanced network activity, the pro-survival effects of 4AP might arise from the increased synaptic NMDAR activation[25], which might trigger neuroprotective effects such as increased BDNF expression[67] and peroxide detoxification in neurons[24]. Thus, improved survival of interneurons in general or an increased ratio of PV+ interneurons will both result in higher responder rates.

There is a general agreement that NMDAR and redox dysfunction underlies the altered gamma oscillations in schizophrenia. In our hands, the initial and transient increase in the power of gamma oscillations together with the immediate decrease in PV expression elicited by GSH-depletion contrast with the sustained drop in gamma oscillation frequency and the late onset of PV loss observed after NMDAR inhibition. This suggests that NMDAR inhibition and GSH-depletion lead to divergent network and PV+ interneuron alterations, which might coexist but are not necessarily interdependent in the schizophrenia pathology.

Methods

Preparation of organotypic hippocampal slice cultures. Animal care and handling was in accordance with the Helsinki declaration and institutional guidelines (https://experimentelle-medizin.charite.de/). Slice culture preparation was proved by the State Office of Health and Social Affairs Berlin (https://www.berlin.de/lageso/), under the license number T0123/11. Data were obtained from ca. 750 brain slices from 150 animals. Each preparation included two animals and the slices were not differentiated between individuals. Slice cultures were prepared and maintained according to the Stoppini method[68]. Briefly, hippocampi from rats expressing venus-YFP on the VGAT promoter[30] were extracted at postnatal day 6–7. Isolated hippocampi were aligned and cut into 400 µm slices perpendicular to the dorsoventral axis with a McIllvain Tissue Chopper. Slices were seeded on PTFE membranes (Millicell-CM, Millipore) and maintained in six-well plates filled with 1 mL culture medium (50% MEM, 25% HBSS, 25% Horse Serum and 1 mM L-glutamine, pH set to 7.3) in a humidified CO_2 incubator (5% CO_2) and left to recover for a day before any treatment.

Pharmacology. Cultures were left to recover for a day after preparation. Drug application was started at DIV1 and was renewed with each change of medium (3 times per week) until the assessment time points (DIV3, 10 or 15). NMDAR inhibition was induced by DL-2-Amino-5-phosphonopentanoic acid (APV) (50 µM; Tocris), which has been shown to completely abolish NMDAR mediated responses in our preparation[69]. Induction of oxidative stress was achieved by co-application of the γ-glutamylcysteine synthetase inhibitor L-Buthionine sulfoximine (BSO, 0.5, 1, 5, 10 µM, Sigma-Aldrich), and by the thioredoxin reductase blocker Auranofin (Au, 1 µM; Sigma). Enhancement of network activity was induced with 4-Aminopyridine (4AP, 100 µM; Tocris), a non-selective blocker of voltage-activated K^+ channels.

Immunohistochemistry. Slice cultures were fixed with 4% paraformaldehyde/4% sucrose in phosphate-buffered saline (PBS) 0.1 M overnight at 4 °C and stored in 30% sucrose/PBS. For immunolabelling, slices were carefully detached from the PTFE membranes and processed free-floating. Incubation with a mouse derived anti-parvalbumin antibody (1:1000; Millipore) in 0.1% Triton X-100/PBS for 3 nights was followed by incubation over 24 hours with a goat anti-mouse Cy3 secondary antibody (1:100; Millipore). Slices were mounted on gold-coated slides and coverslipped with Vectashield HardSet Mounting Medium.

Image acquisition. Fluorescence images were obtained with a spinning disk confocal microscope (Andor Revolution, BFIOptilas GmbH, Gröbenzell, Germany), equipped with an EMCCD camera (Andor iXonEM+), by using the 405, 491, and 561 nm laser lines for mBCI, YFP and Cy3, respectively. Z-stacks were obtained with 20× and 60× objectives (N.A. 0.5 and 1). Panorama images and cell quantification were conducted in 3D reconstructions created with ImageJ (Fiji release 1.51; Wayne Rasband, NIH, USA). Multicolor whole slice reconstructions were made with a NIKON A1R MP multiphoton microscope (25× N.A. 1.1 objective, Nikon, Amsterdam, The Netherlands) at the AMBIO Life Cell Imaging Core Facility (AMBIO.charite.de). Reconstructions of the hippocampal slices were made from tile scans (5 × 4 tiles, 10% overlap for the fitting algorhythm) covering the entire DG and cornu ammonis. The distance between focal planes was kept constant (1.2 µm) while the number of z stacks acquired varied depending on the thickness of the slices.

GSH fluorescence quantification. Hippocampal slices were incubated for exactly 30 min with 50 µM monochlorobimane (mBCI), containing serum free medium, harvested from the PTFE membranes (9–18 slice cultures from 3–4 rats per treatment), followed by rapid freezing in liquid nitrogen. Cell lysates were obtained and the amount of protein was quantified by BSA assay and confirmed by Coomassie dye staining on a SDS-page gel loaded with 5 µg protein homogenate, as described elsewhere[70]. mBCI fluorescence – expressed as mean fluorescence units (MFUs) - was determined in a 96 well plate loaded with 50 µg protein homogenate in a Synergy HT microplate reader (Biotek) using 360 nm excitation and 528 nm emission over time (5–120 min). No difference of the outcome was observed over time.

Oxidized protein quantification. Protein oxidation was measured by oxyblot assay (OxyBlot Protein Oxidation Detection Kit, Merck Chemicals), which labels the carbonyl groups introduced into proteins by oxidative reaction, by analyzing 7 µg protein homogenate and following the manufacture protocol. The densitometric analysis of the staining between 40 and 130 kDa was carried out with QuantityOne Software. Between 3 and 6 oxyblots were performed for each experiment, and their mean was used for further statistical analyses. To control the loading of equal amount of proteins in the representative oxyblot shown in Supplementary Fig. 2b, we performed a western blot assay on a 12% SDS-PAGE gel staining the α4 subunit of proteasome, as described elsewhere[70].

Electrophysiology. The recording chambers were perfused with gassed (95% O_2, 5% CO_2, 1.3 ml per minute) artificial cerebrospinal fluid (aCSF) (in mM: NaCl 129, KCl 3, NaH_2PO_4 1.25, $MgSO_4$ 1.8, $CaCl_2$ 1.6, $NaHCO_3$ 26, glucose 10, pH 7.3). For submerged intracellular recordings, VGAT-YFP positive interneurons were identified using a NoranOz argon laser scanning confocal microscope (Prairie Technologies Inc. Middletown, WI) equipped with a 60× water-immersion objective. Glass micropipettes, filled with intracellular solution (in mM: K-gluconate 135, NaCl 4, $CaCl_2$ 0,05, HEPES 10, EGTA 1, Mg-ATP 2) were used. Whole-cell patch clamp recordings were obtained using a Digidata 1320 digitizer, MultiClamp 700B amplifier and pCLAMP10 software, Molecular Devices (Sunnyvale, CA). Junction potential of −12 mV was not compensated for online. Access resistance (Ra), membrane resistance (Rm), membrane capacitance (Cm) and resting membrane potential (Em) were determined in voltage clamp (VC) mode. In current clamp (CC), pipette resistance was automatically compensated in the bridge balance mode. Consecutively increasing current steps of 25 pA and 1 s duration were applied

and the evoked AP-trains evaluated. Discrimination of adapting and non-adapting interneurons were based on the interevent interval of the first and last 5 APs in a sequence. Individual AP properties were calculated from the second to last AP in a sequence upon a current step of 150 pA.

Local field potentials were recorded in Haas-type recording chamber using a EXB-EXT-02B NPI Electronic amplifier (Norbert Polder Instruments, Germany), high-pass filtered at 0.1 Hz, low-pass filtered at 1 kHz and sampled at 5 kHz by a digitizer CED Micro1401-2 with a ADC12 extension (Cambridge Electronic Design Limited, Cambridge, UK)[71]. Gamma oscillations were induced by adding Cch (5 µM) to the perfusion after 1000 s baseline and recorded from the CA3 pyramidal layer with glass pipettes filled with aCSF (<4 MΩ).

Evaluation and statistics. Data processing of local field potential recordings was done using Spike2 (CED, Cambridge Electronic Design Limited, Cambridge, UK) and Matlab (The MathWorks Inc., 2013a). We computed the power spectral density of the Cch-induced gamma oscillations using Welch's method on ten-second signal regions with a Hamming window with the length of 8192 samples. The gamma oscillation (20–80 Hz) median of the peak frequency and power was calculated from a 90 minute period (from 2000 to 7400 s) after the oscillation had stabilized. The comparison between groups (medians) was performed using the Kruskal-Wallis independent samples test (for more than two groups) and the Mann-Whitney U test (for two groups) in IBM SPSS Statistics 22 on the peak frequency and power in the 90 min (from 2000–7400 s) recording interval. Gamma oscillation power and frequency are presented in boxplots where the median and interquartile range are shown. For the representation of original traces, a low-pass second order Butterworth filter (500 Hz) was applied. The displayed power spectra were obtained from a 120 s interval where the 49–51 Hz frequency range was excluded. The analysis of the different activity patterns is presented as percentage, where the total number of recorded slices, including those displaying uninterrupted gamma oscillations, discontinuous gamma oscillations and no oscillations upon Cch application, are considered as 100%. Slice activity patterns were categorized as follows: gamma refers to slices displaying uninterrupted gamma oscillations in the 2000–7400 s (90 min) recording interval, partial gamma include those slices with discontinuous gamma oscillations during the same time interval and non-responder slices displayed basal activity but no gamma oscillations. The statistical analysis of the responder rates was performed using the two-tailed Fisher's exact test taking into account the three categories of electrophysiological activity.

The quantification of the number of YFP+ (and PV+) interneurons was carried out in 3D reconstructions of the complete hippocampal slice using Arivis Vision 4D (arivis AG, Unterschleissheim, Germany) and its blob-finder analysis operator. For the images obtained with the confocal spinning disk microscope reported as part of Fig. 2c (P0, DIV15, P21/22), the stitching plugin of S. Preibisch *et al.*[72] was used to create the hippocampal panorama pictures. On these reconstructions, PV+ interneurons were counted by hand using the Cell Counter plugin for Fiji (Madison, Wisconsin, USA) based on 64 bit ImageJ distribution (Wayne Rasband, NIH), while VGAT-YFP interneurons were counted using the Analyze Particles plugin.

As the thickness of the cultures varied from slice to slice, we decided to normalize the total number of YPF+ and PV+ interneurons by dividing them with the number of focal planes necessary to scan the entire z-depth from top to bottom (all regions of the hippocampus included). In the figures, the median of the YFP+ and PV+ interneurons per focal plane are presented. However, the ratio of PV+/YFP+ interneurons within a given slice culture was calculated considering the entire slice (all focal planes) and the total YFP+ and PV+ interneuron count. For each treatment and developmental time-point 10 to 20 hippocampal slices obtained from 3–10 rats were analyzed. Size variations in X-Y directions between individual cultures were kept at a minimum due to the alignment of the hippocampi during the preparation. Equal distribution of PV+ cells along the dorsoventral axis of the hippocampus was verified in cultures sliced parallel to the length axis. Statistical evaluation was performed using the Mann-Whitney U test in IBM SPSS version 22.

To assess the GSH and oxidized protein levels, the mean and SD of different experiments were obtained merging slices derived from different rats (n = 3–4 for each experiment and treatment). The significant differences between groups are reported as p values, and were computed by One-way Anova test by applying the Bonferroni correction method for multiple comparisons. Data were tested for normality distribution and homoscedasticity by Shapiro-Wilk and Levene tests, respectively.

Data availability. The datasets generated and analyzed during the current study are available from the corresponding author on reasonable request.

References

1. Hardingham, G. E. & Do, K. Q. Linking early-life NMDAR hypofunction and oxidative stress in schizophrenia pathogenesis. *Nat. Rev. Neurosci.* **17**, 125–134, https://doi.org/10.1038/nrn.2015.19 (2016).
2. Schulz, S. B. *et al*. First and second generation antipsychotics influence hippocampal gamma oscillations by interactions with 5-HT3 and D3 receptors. *Br. J. Pharmacol.* **167**, 1480–1491, https://doi.org/10.1111/j.1476-5381.2012.02107.x (2012).
3. Uhlhaas, P. J. & Singer, W. Abnormal neural oscillations and synchrony in schizophrenia. *Nat. Rev. Neurosci.* **11**, 100–113, https://doi.org/10.1038/nrn2774 (2010).
4. Gonzalez-Burgos, G., Fish, K. N. & Lewis, D. A. GABA Neuron Alterations, Cortical Circuit Dysfunction and Cognitive Deficits in Schizophrenia. *Neural Plasticity*, 1–24, https://doi.org/10.1155/2011/723184 (2011).
5. Traub, R. D., Whittington, M. A., Colling, S. B., Buzsáki, G. & Jefferys, J. G. Analysis of gamma rhythms in the rat hippocampus *in vitro* and *in vivo*. *J. Physiol.* **493**, 471–484 (1996).
6. Fisahn, A., Pike, F. G., Buhl, E. H. & Paulsen, O. Cholinergic induction of network oscillations at 40 Hz in the hippocampus *in vitro*. *Nature* **394**, 186–189, https://doi.org/10.1038/28179 (1998).
7. Bartos, M. *et al*. Fast synaptic inhibition promotes synchronized gamma oscillations in hippocampal interneuron networks. *Proc. Natl. Acad. Sci. USA* **99**, 13222–13227, https://doi.org/10.1073/pnas.192233099 (2002).
8. Bartos, M., Vida, I. & Jonas, P. Synaptic mechanisms of synchronized gamma oscillations in inhibitory interneuron networks. *Nat. Rev. Neurosci.* **8**, 45–56, https://doi.org/10.1038/nrn2044 (2007).

9. Hájos, N. *et al*. Spike timing of distinct types of GABAergic interneuron during hippocampal gamma oscillations *in vitro*. *J. Neurosci.* **24**, 9127–9137, https://doi.org/10.1523/JNEUROSCI.2113-04.2004 (2004).
10. Middleton, S. *et al*. NMDA receptor-dependent switching between different gamma rhythm-generating microcircuits in entorhinal cortex. *Proc. Natl. Acad. Sci. USA* **105**, 18572–18577, https://doi.org/10.1073/pnas.0809302105 (2008).
11. Craig, M. T. & McBain, C. J. Fast Gamma Oscillations Are Generated Intrinsically in CA1 without the Involvement of Fast-Spiking Basket Cells. *J. Neurosci.* **35**, 3616–3624, https://doi.org/10.1523/JNEUROSCI.4166-14.2015 (2015).
12. Lasztóczi, B. & Klausberger, T. Layer-Specific GABAergic Control of Distinct Gamma Oscillations in the CA1 Hippocampus. *Neuron* **81**, 1126–1139, https://doi.org/10.1016/j.neuron.2014.01.021 (2014).
13. Do, K. Q., Cabungcal, J. H., Frank, A., Steullet, P. & Cuenod, M. Redox dysregulation, neurodevelopment, and schizophrenia. *Curr. Opin. Neurobiol.* **19**, 220–230, https://doi.org/10.1016/j.conb.2009.05.001 (2009).
14. Powell, S. B., Sejnowski, T. J. & Behrens, M. M. Behavioral and neurochemical consequences of cortical oxidative stress on parvalbumin-interneuron maturation in rodent models of schizophrenia. *Neuropharmacology* **62**, 1322–1331, https://doi.org/10.1016/j.neuropharm.2011.01.049 (2012).
15. Belforte, J. E. *et al*. Postnatal NMDA receptor ablation in corticolimbic interneurons confers schizophrenia-like phenotypes. *Nat. Neurosci.* **13**, 76–83, https://doi.org/10.1038/nn.2447 (2010).
16. Korotkova, T., Fuchs, E. C., Ponomarenko, A., von Engelhardt, J. & Monyer, H. NMDA receptor ablation on parvalbumin-positive interneurons impairs hippocampal synchrony, spatial representations, and working memory. *Neuron* **68**, 557–569, https://doi.org/10.1016/j.neuron.2010.09.017 (2010).
17. Behrens, M. M. *et al*. Ketamine-induced loss of phenotype of fast-spiking interneurons is mediated by NADPH-oxidase. *Science* **318**, 1645–1647, https://doi.org/10.1126/science.1148045 (2007).
18. Cabungcal, J. H. *et al*. Juvenile antioxidant treatment prevents adult deficits in a developmental model of schizophrenia. *Neuron* **83**, 1073–1084, https://doi.org/10.1016/j.neuron.2014.07.028 (2014).
19. Gysin, R. *et al*. Impaired glutathione synthesis in schizophrenia: convergent genetic and functional evidence. *Proc. Natl. Acad. Sci. USA* **104**, 16621–16626, https://doi.org/10.1073/pnas.0706778104 (2007).
20. Berk, M. *et al*. N-acetyl cysteine as a glutathione precursor for schizophrenia -a double-blind, randomized, placebo-controlled trial. *Biol. Psychiatry* **64**, 361–368, https://doi.org/10.1016/j.biopsych.2008.03.004 (2008).
21. Tosic, M. *et al*. Schizophrenia and oxidative stress: glutamate cysteine ligase modifier as a susceptibility gene. *Am. J. Hum. Genet.* **79**, 586–592, https://doi.org/10.1086/507566 (2006).
22. Steullet, P. *et al*. Redox dysregulation affects the ventral but not dorsal hippocampus: impairment of parvalbumin neurons, gamma oscillations, and related behaviors. *J. Neurosci.* **30**, 2547–2558, https://doi.org/10.1523/JNEUROSCI.3857-09.2010 (2010).
23. Volman, V., Behrens, M. M. & Sejnowski, T. J. Downregulation of parvalbumin at cortical GABA synapses reduces network gamma oscillatory activity. *J. Neurosci.* **31**, 18137–18148, https://doi.org/10.1523/JNEUROSCI.3041-11.2011 (2011).
24. Baxter, P. S. *et al*. Synaptic NMDA receptor activity is coupled to the transcriptional control of the glutathione system. *Nat. Commun.* **6**, 6761, https://doi.org/10.1038/ncomms7761 (2015).
25. Cohen, S. M., Tsien, R. W., Goff, D. C. & Halassa, M. M. The impact of NMDA receptor hypofunction on GABAergic neurons in the pathophysiology of schizophrenia. *Schizophr. Res.* **167**, 98–107, https://doi.org/10.1016/j.schres.2014.12.026 (2015).
26. Vogt Weisenhorn, D. M., Celio, M. R. & Rickmann, M. The onset of parvalbumin-expression in interneurons of the rat parietal cortex depends upon extrinsic factor(s). *Eur. J. Neurosci.* **10**, 1027–1036 (1998).
27. Gorba, T., Klostermann, O. & Wahle, P. Development of neuronal activity and activity-dependent expression of brain-derived neurotrophic factor mRNA in organotypic cultures of rat visual cortex. *Cereb. Cortex* **9**, 864–877 (1999).
28. Jiang, M. & Swann, J. W. A role for L-type calcium channels in the maturation of parvalbumin-containing hippocampal interneurons. *Neuroscience* **135**, 839–850, https://doi.org/10.1016/j.neuroscience.2005.06.073 (2005).
29. Dupont, J.-L., Fourcaudot, E., Beekenkamp, H., Poulain, B. & Bossu, J.-L. Synaptic organization of the mouse cerebellar cortex in organotypic slice cultures. *The Cerebellum* **5**, 243–256, https://doi.org/10.1080/14734220600905317 (2006).
30. Uematsu, M. *et al*. Quantitative chemical composition of cortical GABAergic neurons revealed in transgenic venus-expressing rats. *Cereb. Cortex* **18**, 315–330, https://doi.org/10.1093/cercor/bhm056 (2008).
31. Nitsch, R., Bergmann, I., Küppers, K., Mueller, G. & Frotscher, M. Late appearance of parvalbumin-immunoreactivity in the development of GABAergic neurons in the rat hippocampus. *Neurosci. Lett.* **118**, 147–150 (1990).
32. Doischer, D. *et al*. Postnatal Differentiation of Basket Cells from Slow to Fast Signaling Devices. *J. Neurosci.* **28**, 12956–12968, https://doi.org/10.1523/JNEUROSCI.2890-08.2008 (2008).
33. Kudin, A. P., Augustynek, B., Lehmann, A. K., Kovács, R. & Kunz, W. S. The contribution of thioredoxin-2 reductase and glutathione peroxidase to H(2)O(2) detoxification of rat brain mitochondria. *Biochim. Biophys. Acta* **1817**, 1901–1906, https://doi.org/10.1016/j.bbabio.2012.02.023 (2012).
34. Mandal, P. K. *et al*. System x c – and Thioredoxin Reductase 1 Cooperatively Rescue Glutathione Deficiency. *J. Biol. Chem.* **285**, 22244–22253, https://doi.org/10.1074/jbc.M110.121327 (2010).
35. Ruszkiewicz, J. & Albrecht, J. Changes of the Thioredoxin System, Glutathione Peroxidase Activity and Total Antioxidant Capacity in Rat Brain Cortex During Acute Liver Failure: Modulation by l-histidine. *Neurochem. Res.* **40**, 293–300, https://doi.org/10.1007/s11064-014-1417-9 (2015).
36. Dringen, R., Brandmann, M., Hohnholt, M. C. & Blumrich, E.-M. Glutathione-Dependent Detoxification Processes in Astrocytes. *Neurochem. Res.* **40**, 2570–2582, https://doi.org/10.1007/s11064-014-1481-1 (2015).
37. Reynolds, G. P. & Neill, J. C. Modelling the cognitive and neuropathological features of schizophrenia with phencyclidine. *J. Psychopharmacol. (Oxford)* **30**, 1141–1144, https://doi.org/10.1177/0269881116667668 (2016).
38. Wang, C. Z., Yang, S. F., Xia, Y. & Johnson, K. M. Postnatal phencyclidine administration selectively reduces adult cortical parvalbumin-containing interneurons. *Neuropsychopharmacology* **33**, 2442–2455, https://doi.org/10.1038/sj.npp.1301647 (2008).
39. Papadia, S. *et al*. Synaptic NMDA receptor activity boosts intrinsic antioxidant defenses. *Nat. Neurosci.* **11**, 476–487, https://doi.org/10.1038/nn2071 (2008).
40. Kovács, R. *et al*. Free radical-mediated cell damage after experimental status epilepticus in hippocampal slice cultures. *J. Neurophysiol.* **88**, 2909–2918, https://doi.org/10.1152/jn.00149.2002 (2002).
41. Albus, K., Wahab, A. & Heinemann, U. Standard antiepileptic drugs fail to block epileptiform activity in rat organotypic hippocampal slice cultures. *Br. J. Pharmacol.* **154**, 709–724, https://doi.org/10.1038/bjp.2008.112 (2008).
42. Albus, K., Heinemann, U. & Kovács, R. Network activity in hippocampal slice cultures revealed by long-term *in vitro* recordings. *J. Neurosci. Methods* **217**, 1–8, https://doi.org/10.1016/j.jneumeth.2013.04.014 (2013).
43. Miller, M. N., Okaty, B. W., Kato, S. & Nelson, S. B. Activity-dependent changes in the firing properties of neocortical fast-spiking interneurons in the absence of large changes in gene expression. *Dev. Neurobiol.* **71**, 62–70, https://doi.org/10.1002/dneu.20811 (2011).
44. Dehorter, N. *et al*. Tuning of fast-spiking interneuron properties by an activity-dependent transcriptional switch. *Science* **349**, 1216–1220, https://doi.org/10.1126/science.aab3415 (2015).
45. Jadi, M. P., Behrens, M. M. & Sejnowski, T. J. Abnormal Gamma Oscillations in N-Methyl-D-Aspartate Receptor Hypofunction Models of Schizophrenia. *Biol. Psychiatry* **79**, 716–726, https://doi.org/10.1016/j.biopsych.2015.07.005 (2016).

46. Steullet, P. *et al*. Oxidative stress-driven parvalbumin interneuron impairment as a common mechanism in models of schizophrenia. *Mol. Psychiatry* **22**, 936–943, https://doi.org/10.1038/mp.2017.47 (2017).
47. Pozzo Miller, L. D., Mahanty, N. K., Connor, J. A. & Landis, D. M. Spontaneous pyramidal cell death in organotypic slice cultures from rat hippocampus is prevented by glutamate receptor antagonists. *Neuroscience* **63**, 471–487 (1994).
48. Gutiérrez, R. & Heinemann, U. Synaptic reorganization in explanted cultures of rat hippocampus. *Brain Res.* **815**, 304–316 (1999).
49. Schneider, J. *et al*. A reliable model for gamma oscillations in hippocampal tissue. *J. Neurosci. Res.* **93**, 1067–1078, https://doi.org/10.1002/jnr.23590 (2015).
50. Rompala, G. R., Zsiros, V., Zhang, S., Kolata, S. M. & Nakazawa, K. Contribution of NMDA receptor hypofunction in prefrontal and cortical excitatory neurons to schizophrenia-like phenotypes. *Plos One* **8**, e61278, https://doi.org/10.1371/journal.pone.0061278 (2013).
51. Jiang, Z., Cowell, R. M. & Nakazawa, K. Convergence of genetic and environmental factors on parvalbumin-positive interneurons in schizophrenia. *Front. Behav. Neurosci.* **7**, 116, https://doi.org/10.3389/fnbeh.2013.00116 (2013).
52. Cabungcal, J.-H. *et al*. Glutathione deficit during development induces anomalies in the rat anterior cingulate GABAergic neurons: Relevance to schizophrenia. *Neurobiol. Dis.* **22**, 624–637, https://doi.org/10.1016/j.nbd.2006.01.003 (2006).
53. Schiavone, S. *et al*. Involvement of NOX2 in the development of behavioral and pathologic alterations in isolated rats. *Biol. Psychiatry* **66**, 384–392, https://doi.org/10.1016/j.biopsych.2009.04.033 (2009).
54. Schiavone, S. *et al*. NADPH oxidase elevations in pyramidal neurons drive psychosocial stress-induced neuropathology. *Transl. Psychiatry* **2**(5), e111, https://doi.org/10.1038/tp.2012.36 (2012).
55. Behrens, M. M. & Sejnowski, T. J. Does schizophrenia arise from oxidative dysregulation of parvalbumin-interneurons in the developing cortex? *Neuropharmacology* **57**, 193–200, https://doi.org/10.1016/j.neuropharm.2009.06.002 (2009).
56. Gysin, R. *et al*. Genetic dysregulation of glutathione synthesis predicts alteration of plasma thiol redox status in schizophrenia. *Antioxid. Redox Signal.* **15**, 2003–2010, https://doi.org/10.1089/ars.2010.3463 (2011).
57. Cabungcal, J.-H., Steullet, P., Kraftsik, R., Cuenod, M. & Do, K. Q. Early-life insults impair parvalbumin interneurons via oxidative stress: reversal by N-acetylcysteine. *Biol. Psychiatry* **73**, 574–582, https://doi.org/10.1016/j.biopsych.2012.09.020 (2013).
58. Ibi, M. *et al*. Depressive-Like Behaviors Are Regulated by NOX1/NADPH Oxidase by Redox Modification of NMDA Receptor 1. *The Journal of Neuroscience* **37**, 4200–4212, https://doi.org/10.1523/JNEUROSCI.2988-16.2017 (2017).
59. Köhr, G., Eckardt, S., Lüddens, H., Monyer, H. & Seeburg, P. H. NMDA receptor channels: subunit-specific potentiation by reducing agents. *Neuron* **12**, 1031–1040 (1994).
60. Steullet, P., Neijt, H. C., Cuénod, M. & Do, K. Q. Synaptic plasticity impairment and hypofunction of NMDA receptors induced by glutathione deficit: relevance to schizophrenia. *Neuroscience* **137**, 807–819, https://doi.org/10.1016/j.neuroscience.2005.10.014 (2006).
61. Dean, O., Bush, A. I., Berk, M., Copolov, D. L. & van den Buuse, M. Interaction of glutathione depletion and psychotropic drug treatment in prepulse inhibition in rats and mice. *Pharmacol. Biochem. Behav.* **97**, 293–300, https://doi.org/10.1016/j.pbb.2010.08.013 (2010).
62. Castagné, V., Rougemont, M., Cuenod, M. & Do, K. Q. Low brain glutathione and ascorbic acid associated with dopamine uptake inhibition during rat's development induce long-term cognitive deficit: relevance to schizophrenia. *Neurobiol. Dis.* **15**, 93–105 (2004).
63. Baxter, P. S. & Hardingham, G. E. Adaptive regulation of the brain's antioxidant defences by neurons and astrocytes. *Free Radic. Biol. Med.* **100**, 147–152, https://doi.org/10.1016/j.freeradbiomed.2016.06.027 (2016).
64. Cabungcal, J.-H. *et al*. Perineuronal nets protect fast-spiking interneurons against oxidative stress. *Proc. Natl. Acad. Sci. USA* **110**, 9130–9135, https://doi.org/10.1073/pnas.1300454110 (2013).
65. Hensch, T. K. & Fagiolini, M. Excitatory-inhibitory balance and critical period plasticity in developing visual cortex. *Prog. Brain Res.* **147**, 115–124, https://doi.org/10.1016/S0079-6123(04)47009-5 (2005).
66. Carulli, D. *et al*. Animals lacking link protein have attenuated perineuronal nets and persistent plasticity. *Brain* **133**, 2331–2347 (2010).
67. Hardingham, G. E., Fukunaga, Y. & Bading, H. Extrasynaptic NMDARs oppose synaptic NMDARs by triggering CREB shut-off and cell death pathways. *Nat. Neurosci.* **5**, 405–414, https://doi.org/10.1093/brain/awq145 (2002).
68. Stoppini, L., Buchs, P. A. & Muller, D. A simple method for organotypic cultures of nervous tissue. *J. Neurosci. Methods* **37**, 173–182 (1991).
69. Liotta, A. *et al*. Energy demand of synaptic transmission at the hippocampal Schaffer-collateral synapse. *J. Cereb. Blood Flow Metab.* **32**, 2076–2083, https://doi.org/10.1038/jcbfm.2012.116 (2012).
70. Mishto, M. *et al*. The immunoproteasome α5i subunit is a key contributor to ictogenesis in a rat model of chronic epilepsy. *Brain, Behavior, and Immunity* **49**, 188–196, https://doi.org/10.1016/j.bbi.2015.05.007 (2015).
71. Lemercier, C. E., Schulz, S. B., Heidmann, K. E., Kovács, R. & Gerevich, Z. Dopamine D3 Receptors Inhibit Hippocampal Gamma Oscillations by Disturbing CA3 Pyramidal Cell Firing Synchrony. *Front. Pharmacol.* **6**, 297, https://doi.org/10.3389/fphar.2015.00297 (2015).
72. Preibisch, S., Saalfeld, S. & Tomancak, P. Globally optimal stitching of tiled 3D microscopic image acquisitions. *Bioinformatics* **25**, 1463–1465, https://doi.org/10.1093/bioinformatics/btp184 (2009).

Acknowledgements

The study was supported by the DFG grant Ko3814/1-1 to L.A.H.H., G.C.G. and R.K.

Author Contributions

L.A.H.H. and C.K. investigated the effects on gamma oscillations, G.C.G. conducted the patch clamp experiments and analysis, L.A.H.H. performed the immunofluorescent analysis of the cultures, M.M. was responsible for the G.S.H. determination, L.A.H.H., Z.G., J.R.P.G., R.K. were involved in the design and analysis of the study and all authors contributed to writing the manuscript.

Additional Information

Supplementary information accompanies this paper at https://doi.org/10.1038/s41598-018-27830-2.

Competing Interests: The authors declare no competing interests.

Publisher's note: Springer Nature remains neutral with regard to jurisdictional claims in published maps and institutional affiliations.

Curriculum Vitae

My curriculum vitae does not appear in the electronic version of my paper for reasons of data protection.

List of publications

Hasam-Henderson, L.A., Gotti, G.C., Mishto, M., Klisch, C., Gerevich, Z., Geiger, J.R.P., and Kovács, R. NMDA-receptor inhibition and oxidative stress during hippocampal maturation differentially alter parvalbumin expression and gamma-band activity. Scientific Reports, 8, (2018).

Acknowledgments

First, I want to thank my supervisor Dr. Richard Kovács for guiding me in this life quest. I will always be grateful for his trust and patience.

I want to thank Prof. Geiger for hosting me in his institute, for sharing his knowledge, and for the efforts made to provide financial support, together with Dr. Gerevich, that allowed me to finish my studies.

I want to thank Dr. Gerevich for giving me the chance to join his group and for being flexible with my scientific interests.

I want to thank Grace Gotti for being a great team player and for all the hours she invested in this project.

I want to thank Dr. Jan Schmoranzer for helping me to find more efficient ways to perform the image analysis.

I am grateful to Prof. Henrik Alle for his guidance in difficult times.

I am also thankful to the people that were part of my lab-life: to Constantin Klisch for the company during the long experimental days, to Stephanie Schinkel for introducing me to the world of immunohistochemistry, to Andrea Wilke for sharing her experience and knowledge with me; to Victoria Antemann, Vera Wuntke and Stephanie Braud for their help and support.

I want to thank Sonja Frosinski and Katrin Schulze for always finding the time to help me in all administrative matters and for their kindness without end.

From the Medical Neuroscience office, I want to thank Dr. Benedikt Salmen for being there for me every time, Ralf Ansorg for always helping me in the administrative steps, and Julia Rummel and Ekaterina Lyras for all the administrative support.

I also want to thank Pamela Glowacki and Franziska Grimm from the Welcome Center of the Charité for taking care of my visa procedures always efficiently and in the most friendly way.

To Linda Brenndörfer for her endless help with my German and teaching assignments.

To my life companion, Patricio López-Serrano, for embarking on Matlab analysis quests with me, for listening patiently to all my thoughts and ideas, for learning what an interneuron is, and finding ways to remember the details of my experiments. For pushing me out of my comfort zone and for never losing trust in me.

To my parents, Frieda Henderson and Steven Hasam, for teaching me that real love means to be critical and constructive. For constantly pushing me forward, for listening and being there all the time despite the distance.

To my grandmother, Maria Lengyel, for sharing her wisdom, for teaching me to find new angles on life, and for making possible everything that followed my learning English.